RWTH Aachen University
Physics Institute III B
Forschungszentrum Jülich
Institute for Nuclear Physics IV

Master Thesis

Comparison of Frozen and Quasi Frozen Spin Concepts for a Deuteron Electrical Dipole Moment Storage Ring

Author: Alexander Albert Skawran

Supervisor: Prof. Dr. rer. nat. Andreas Lehrach

Submission Date: 28 September 2016

Abstract

The purpose of the Jülich Electric Dipole moment Investigations (JEDI) collaboration is the measurement of the electric dipole moment of charged particles like proton or deuteron. There are two possible experimental setups for the realisation of this measurement with deuterons: The Frozen and Quasi Frozen Spin storage ring experiments. Both approaches are discussed and compared in this thesis. Various misalignments and systematic effects are simulated in the context of comparison. Furthermore the clockwise-counterclockwise method (CW-CCW) is applied and checked for its validity.

Abstrakt

Das Ziel der Jülich Electric Dipole moment Investigations (JEDI) Kollaboration ist die Messung des elektrischen Dipolmomentes von geladen Teilchen wie dem Proton oder dem Deuteron. Es existieren zwei mögliche Aufbauten für ein Experiment mit Deuteronen: Die sogenannten Frozen- und Quasi-Frozen-Spin-Speicherringexperimente. Beide Ansätze werden in dieser Arbeit diskutiert und verglichen. Verschiedene Ausrichtungsfehler und systematischen Effekte werden für diesen Vergleich simuliert. Des Weiteren wird die Clockwise-Counterclockwise-Methode (CW-CCW) angewendet und auf die Einsetzbarkeit überprüft.

Contents

List of Figures v

List of Tables vii

1 Introduction 1
- 1.1 Task . . . 1
- 1.2 Structure of Thesis . . . 2

2 Scientific Motivations and Spin Motion 3
- 2.1 Electric Dipole Moment . . . 3
  - 2.1.1 Definition and $\mathcal{CP}$ Violation . . . 3
- 2.2 Thomas-BMT Equation and Measurement of an EDM . . . 5
  - 2.2.1 Thomas BMT Equation for Storage Ring Experiments . . . 5
  - 2.2.2 Influence of Gravitation . . . 8
  - 2.2.3 Comoving Coordinate System . . . 9
  - 2.2.4 Spin Tune . . . 9
  - 2.2.5 Spin Coherence Time . . . 10
  - 2.2.6 Period of Measurement . . . 10

3 Applied Methods and Systematic Effects 13
- 3.1 Frozen Spin Ring . . . 13
  - 3.1.1 Suitable Particles for the Frozen Spin Experiment . . . 14
  - 3.1.2 Properties of Frozen Spin Lattice . . . 15
- 3.2 Quasi Frozen Spin Ring . . . 17
  - 3.2.1 Properties of Simulated Quasi Frozen Spin Lattice . . . 19
- 3.3 Sources of Artificial Vertical Spin Build Up . . . 20
  - 3.3.1 Transverse Magnetic and Vertical Electric Fields . . . 20
  - 3.3.2 Gradient Effect . . . 22
  - 3.3.3 Longitudinal Magnetic and Electric Fields . . . 25
  - 3.3.4 Gravitation . . . 25
  - 3.3.5 Spin Invariant Axis . . . 26
- 3.4 Clockwise Counterclockwise Method . . . 26
  - 3.4.1 Counterclockwise Method Gradient Fields . . . 27
  - 3.4.2 Counterclockwise Method Gravitation . . . 28

3.4.3 Counterclockwise Method Overview 28

4 Utilized Simulation Programs and Software Extensions 29

4.1 COSY INFINITY 29

4.2 COSY Toolbox 30

4.3 Modifications to COSY Toolbox 30

4.3.1 E×B Deflectors 30

4.3.2 Fringe Fields 32

4.3.3 Calculator for Ring Properties 33

4.3.4 Spin Analysis 34

4.3.5 List of Ring Elements 35

4.3.6 Sector and Rectangular Bending Magnets 35

4.4 Ring Lattices 36

5 Simulation Results 37

5.1 Spin Tune 37

5.1.1 Frozen Spin 37

5.1.2 Quasi Frozen Spin 38

5.1.3 Statistical Error 38

5.2 Simulation of Misalignments 41

5.2.1 Misalignments of Deflectors 41

5.2.2 Misalignments of Quadrupoles 46

5.3 Clockwise Counterclockwise 49

5.3.1 Misalignments of Deflectors 50

5.3.2 Misalignments of Quadrupoles 54

6 Summary and Outlook 59

Bibliography 61

7 Statutory Declaration / Eidesstattliche Versicherung 67

List of Figures

2.1 A comoving coordinate system where the black line symbolizes an arbitrary beam path in an accelerator. 9

3.1 The simulated Frozen Spin ring lattice. 16
3.2 The simulated Quasi Frozen ring lattice and the corresponding optical functions. 18
3.3 Representation of the used coordinate system inside an E×B deflector. . 21
3.4 Magnetic field inside a quadrupole. At the center of the quadrupole the magnetic field vanishes. 21
3.5 The relative difference for the vertical spin build up with an existing or respectively vanishing gradient field effect inside the quadrupoles. 24

4.1 The generated lattice plot of COTOBO for the Quasi Frozen Ring lattice. 32
4.2 Shape of fringe fields and the device length compared with the effective length. 34

5.1 Vertical spin build up for the simulated Frozen Spin lattice. 39
5.2 Vertical spin build up for the simulated Quasi Frozen Spin lattice. 40
5.3 Vertical spin build up for different magnitudes of EDM and RMS of rotation misalignments of the deflectors around the vertical axis. Each simulation has new randomly generated misalignments. 42
5.4 Vertical spin build up for different magnitudes of EDM and RMS of rotation misalignments of the deflectors around the longitudinal axis. Each simulation has new randomly generated misalignments. 44
5.5 Vertical spin build up for different magnitudes of EDM and RMS of rotation misalignments of the deflectors around the radial axis. Each simulation has new randomly generated misalignments. 45
5.6 Vertical spin build up for different magnitudes of EDM and RMS of shift misalignments of the quadrupoles in vertical direction. Each simulation has new randomly generated misalignments. 47
5.7 Vertical spin build up for different magnitudes of EDM and RMS of shift misalignments of the quadrupoles in radial direction. Each simulation has new randomly generated misalignments. 48

5.8 Frozen Spin - CW-CCW method for rotation misalignments of the E×B deflectors around the vertical axis. 50
5.9 Quasi Frozen Spin - CW-CCW method for rotation misalignments of the deflectors around the vertical axis. 51
5.10 Frozen Spin - CW-CCW method for rotation misalignments of the deflectors around the longitudinal axis. 52
5.11 Quasi Frozen Spin - CW-CCW method for rotation misalignments of the deflectors around the longitudinal axis. 53
5.12 Frozen Spin - CW-CCW method for shift misalignments of the quadrupoles in vertical direction. 54
5.13 Quasi Frozen Spin - CW-CCW method for shift misalignments of the quadrupoles in vertical direction. 55
5.14 Frozen Spin - CW-CCW method for shift misalignments of the quadrupoles in radial direction. 56
5.15 Quasi Frozen - CW-CCW method for shift misalignments of the quadrupoles in radial direction. 57

List of Tables

2.2 Characteristic values of N, f, τ and A. 11

3.1 Anomalous magnetic momentum for different particles. 15
3.2 Properties of the beam in the simulated Frozen Spin ring. 17
3.3 Properties of the beam in the simulated Quasi Frozen Spin ring. 20
3.4 Sign of angular veloticity $\vec{\omega}$ of spin rotation $\frac{d\vec{s}}{dt} = \vec{s} \times \vec{\omega}$ due to different effects. The $'+'$ for the CW method characterises the original direction of $\vec{\omega}$. A $'+'$ of the CCW method represents the same direction of $\vec{\omega}$ for the reversed beam motion and a $'-'$ characterises the opposite motion of $\vec{\omega}$. 28

5.1 Magnitudes of simulated emittances. 37

1 Introduction

One fundamental challenge of modern physics is the explanation of baryogenesis. Charge parity ($\mathcal{CP}$) symmetry violation could be the key to this matter-antimatter asymmetry puzzle [1]. A permanently existing electric dipole moment (EDM) of a subatomic particle could provide such a $\mathcal{CP}$ violation[2]. The Jülich Electric Dipole moment Investigations (JEDI) collaboration at the Institute for Nuclear Physics of the Forschungszentrum Jülich was founded to determine the EDM of deuterons [3]. The plan of the JEDI collaboration is the construction of a storage ring containing for charged particles. The behaviour of the polarization under the influence of electromagnetic fields during a time period deliver information about the EDM. The complexity and requirement of high precision measurment is mainly caused due to the small impact of the EDM on the observables. Thus the avoidance and consideration of many different effects causing disruption e.g. misalignments or gravitation is of great significance. The Storage Ring Electric Dipole Moment Collaboration (srEDM) approved the so called Frozen Spin concept where the polarization of the beam is aligned parallel to the beam motion [4]. An EDM is measured by a vertical change of the polarization. A storage ring needs electromagnetic deflectors to store the beam inside the machine. The Frozen Spin concept requires deflectors including electrical and magnetical fields at once. Due to technical aspects the construction of curved E×B deflectors is a difficult task. Another concept by Y.Senichev [5] avoids the usage of curved E×B deflectors. The second concept is called Quasi Frozen Spin where curved magnetic deflectors and straight E×B devices are used and the polarization orientation oscillates around the beam direction.

1.1 Task

Systematics could feign an EDM signal. In this thesis the effect of different misalignments is analysed and compared for Frozen and Quasi Frozen Spin concepts. Additionally, the effect of gradient fields, fringe fields and gravitation are discussed. The experimental setup also contains elements which can cause a disturbing effect on the polarization for example magnetic quadrupoles. Only commutativity of spin rotations could disturb the Quasi Frozen concept. Hence, it is checked if the Quasi Frozen concept works per se.
A possible way to eliminate misleading effects is the use of the clockwise-counterclockwise method (CW-CCW). In this concept the beams are injected into the ring in the opposite

direction after each cycle. The polarization behaviour depends on the direction of the beam motion. This effect could enable the cancellation of misleading effects and is verified for some effects.
The analysis of misalignments needs simulations using spin tracking. Hence the spin and particle tracking software COSY INFINITY [6] and the C++ based framework COSY Toolbox [7] are used in this thesis. COSY Toolbox was not developed for the analysis of the EDM storage rings and is lacking some tools. Therefore, the COSY Toolbox is extended to enable the simulation of the EDM storage ring experiments. Moreover, it is checked if COSY INFINITY can be applied for simulations regarding the influence of construction accuracy on the spin motion.

1.2 Structure of Thesis

Chapter 2 treats the EDM and the link between EDM and CP violation. The principle of the EDM measurement and the setup of the Frozen and Quasi Frozen Spin concept are explained in Chapter 3. Moreover, the influence of the main systematic effects in a storage ring experiment is considered. Finally the CW-CCW method is explained and examined for different kinds of misalignments. Chapter 4 presents the applied simulation programs and includes the improvements of COSY Toolbox. The simulation results in regard to misalignments and the CW-CCW method are presented in Chapter 5. Chapter 6 summaries and concludes the results of this thesis.

2 Scientific Motivations and Spin Motion

The measured matter antimatter asymmetry in our universe [8]

$$\frac{n_B - n_{\overline{B}}}{n_\gamma} = \left(6.1^{+0.3}_{-0.2} \cdot 10^{-10}\right) \tag{2.1}$$

is an unsolved puzzle. The number density of baryons is n_B, the number density of antibaryons is $n_{\overline{B}}$ and the number density of photons is n_γ. The expectation by the standard model of cosmology (SCM) [9] is

$$\frac{n_B}{n_\gamma} = \frac{n_{\overline{B}}}{n_\gamma} \simeq 10^{-18}. \tag{2.2}$$

Hence, the theoretical expectation is 8 magnitudes smaller than the experimental measurement.
One possible answer to this riddle requires the three Sakharov conditition [1]:

1 The baryon number is violated at the beginning of the universe

2 Charge ($\mathcal{C}$) and parity ($\mathcal{P}$) symmetry is violated

3 During the generation of baryon number, the universe was out of thermal equilibrium.

To support these conditions, experimental evidences of $\mathcal{CP}$ violating processes are needed. One new source would be a permanent electric dipole moment (EDM) of subatomic particles.

2.1 Electric Dipole Moment

2.1.1 Definition and $\mathcal{CP}$ Violation

The EDM is a quantity for the electrical charge separation of an object. In classical physics it is defined by [2]

$$\vec{d} = \sum_i q_i \vec{r}_i \tag{2.3}$$

where q_i is the i-th electrical charge and $\vec{r}_i$ is the i-th displacement vector with respect to the center of the electrical charges. The energy, momentum, mass and if not specified otherwise, all given values are listed in natural units, where $c = \hbar = 1$. However, $\vec{d}$ is a polar vector which is conserved under time ($\mathcal{T}$) but not under $\mathcal{P}$ transformations. In the restframe of subatomic particles the only remaining vector is the spin. Hence the EDM must be redefined [2]

$$\vec{d} = \sum_i q_i \vec{r}_i \rightarrow \frac{\eta}{2} \frac{e}{m} \vec{s}. \tag{2.4}$$

A dimensionless scale factor is η, $\vec{s}$ is the spin of the particle. However the spin behaves like an axial vector which behaves opposite to a polar vector under $\mathcal{P}$- and $\mathcal{T}$ transformations. The third examined symmetry is the $\mathcal{C}$ symmetry.

Apart from the EDM the magnetic dipole moment (MDM) is similar defined with $\vec{\mu} = \frac{g}{2} \frac{e}{m} \vec{s}$, where g is the Landé g-factor. The MDM is in classical physics as well as for sub atomic particles an axial vector.

Considering the Hamiltonian of the MDM and EDM

$$\mathcal{H} = -\vec{\mu} \cdot \vec{B} - \vec{d} \cdot \vec{E}, \tag{2.5}$$

where $\vec{E}$ is the external electric field and $\vec{B}$ is the external magnetic field. When the $\mathcal{P}$ and $\mathcal{T}$ transformations are applied to the Hamiltonian the symmetry is obviously violated:

$$\mathcal{P}(\mathcal{H}) \rightarrow -\vec{\mu} \cdot \vec{B} - \vec{d} \cdot (-\vec{E}) = -\vec{\mu} \cdot \vec{B} + \vec{d} \cdot \vec{E} \neq \pm \mathcal{H} \tag{2.6}$$

$$\mathcal{T}(\mathcal{H}) \rightarrow -(-\vec{\mu}) \cdot (-\vec{B}) - (-\vec{d}) \cdot \vec{E} = -\vec{\mu} \cdot \vec{B} + \vec{d} \cdot \vec{E} \neq \pm \mathcal{H} \tag{2.7}$$

Assuming that the $\mathcal{CPT}$ symmetry is conserved then the $\mathcal{CP}$ symmetry must be violated, if the $\mathcal{T}$ symmetry is broken.

The Standard Model (SM) prediction for EDM of nucleons is in the range of 10^{-33} e cm up to 10^{-31} e cm [10]. Much larger values for the EDM would be a sign for physics beyond the SM. The actual limits are far away of this SM range. Some limits are listed in Table 2.1 [11]. The limit of the electron is deduced from the thallium EDM measurement and the value of the proton is determined by the mercury EDM limit. Hence, the actual limit of the proton EDM is not established by a direct measurement.

Current EDM limit	e	n	p	Tl	Xe	Hg
$\lvert d \rvert$ (e cm)	$1.6 \cdot 10^{-27}$	$3 \cdot 10^{-26}$	$7.9 \cdot 10^{-25}$	$9 \cdot 10^{-25}$	$6 \cdot 10^{-28}$	$3.1 \cdot 10^{-29}$

Table 2.1: Current EDM limits [11].

2.2 Thomas-BMT Equation and Measurement of an EDM

The basic idea to detect an EDM is to apply electromagnetic fields and observe the spin motion. In the restframe of a particle the interaction between the electric and magnetic dipole moment with electromagnetic fields is

$$\frac{d\vec{s}}{dt} = -\vec{\mu} \times \vec{B} - \vec{d} \times \vec{E}. \tag{2.8}$$

Regarding Equation 2.8 an EDM of a particle in rest interacts only with the electric field. For neutral particles like neutrons, traps are constructed where an applied electric field induces a spin motion [12]. These traps cannot be used for electrical charged particles because an electrical field accelerates the particles. Thus storage rings are a possibility to store charged particles and to observe a possibly existing EDM.

2.2.1 Thomas BMT Equation for Storage Ring Experiments

The equation of spin motion of particles in rest 2.8 cannot be used for an accelerator experiment, because the EDM of moving particles also interacts with the magnetic fields in the experiment. Thus extensions of the Equation 2.8 are required. The needed equations can be constructed by equations which are covariant regarding Lorentz transformations. The electromagnetic fields are described by the electromagnetic field tensor $F^{\mu\nu}$:

$$F^{\mu\nu} = \begin{pmatrix} 0 & -E_1 & -E_2 & -E_3 \\ E_1 & 0 & -B_3 & B_2 \\ E_2 & B_3 & 0 & -B_1 \\ E_3 & -B_2 & B_1 & 0 \end{pmatrix}, \hat{F}^{\mu\nu} = \begin{pmatrix} 0 & -B_1 & -B_2 & -B_3 \\ B_1 & 0 & E_3 & -E_2 \\ B_2 & -E_3 & 0 & E_1 \\ B_3 & E_2 & -E_1 & 0 \end{pmatrix} \tag{2.9}$$

where E_i and B_i are the components of the electric field and respectively the components of the magnetic field.[1]

The particle motion is described by

$$m\frac{du_\nu}{d\tau} = qF^{\nu\rho}u_\rho + \frac{\mu}{I}u_\sigma\left(\partial_\nu + u_\nu u^\gamma \partial_\gamma\right)\hat{F}^{\sigma\rho}S_\rho + \frac{d}{I}u_\sigma\left(\partial_\nu + u_\nu u^\gamma \partial_\gamma\right)F^{\sigma\rho}S_\rho \tag{2.10}$$

where u_μ is the four velocity, $S_\mu = (0, -\vec{s})$ is the pseudo spin vector, q is the electrical charge, I is the isospin, τ is the proper time, $\partial_\alpha = \frac{\partial}{\partial x^\alpha}$ and $qF^{\nu\rho}u_\rho$ is the Lorentz force

[1] Some remarks regarding the use of tensors are made. Greek letters are free variable parameters. Latin letters are used for the indices regarding the space parameters $1, 2, 3$.

[13],[14],[15],[16]. The spin motion can be determined by [13],[14],[15],[16] with

$$\begin{aligned}\frac{dS_\nu}{d\tau} = \frac{\mu}{I} F_{\nu\sigma} S^\sigma - \left(\frac{\mu}{I} - \frac{q}{m}\right) u_\nu u_\mu F^{\mu\sigma} S_\sigma + \frac{\mu}{Im} u_\nu u_\mu S^\gamma \partial_\gamma \hat{F}^{\mu\sigma} S_\sigma - \\ \frac{d}{I}\hat{F}_{\nu\sigma} S^\sigma + \frac{d}{I} u_\nu u_\mu \hat{F}^{\mu\sigma} S_\sigma + \frac{d}{Im} u_\nu u_\mu S^\gamma \partial_\gamma F^{\mu\sigma} S_\sigma.\end{aligned} \tag{2.11}$$

This is the Thomas-Bargmann-Michel-Telegdi (Thomas-BMT) equation including the EDM and gradient fields. The source of the gradient effect is the Stern-Gerlach effect [17] where the force on the magnetic dipole moment is given by

$$\vec{F} = \vec{\nabla}\left(\vec{\mu}\cdot\vec{B}\right) \tag{2.12}$$

in the rest frame of the particle. The effect on the EDM is similar

$$\vec{F} = \vec{\nabla}\left(\vec{d}\cdot\vec{E}\right). \tag{2.13}$$

The spin motion with respect to the particle motion is measured in the experiment. The desired motion in an experiment is indicated by the velocity u^2. The spin in this direction is S^2. Hence, the measured spin motion is

$$\frac{d\left(S_{\text{Observed}}\right)_i}{d\tau} = \frac{dS_i}{d\tau} - \frac{du_i^2}{d\tau} S^2/u^2. \tag{2.14}$$

Finally the spin motion can be described by rotations of the part caused by the MDM and the EDM. Neglecting the terms including ∂_γ the spin motion is [16]:

$$\frac{d\vec{s}}{dt} = \vec{s}\times\left(\vec{\omega}_\mu + \vec{\omega}_{EDM}\right) = \vec{s}\times\left[\underbrace{\frac{\mu}{I\gamma}\vec{R} - \frac{e}{m}\vec{N}}_{\vec{\omega}_\mu} + \underbrace{\frac{d}{I\gamma}\vec{\tilde{R}}}_{\vec{\omega}_{EDM}}\right] \tag{2.15}$$

$$\vec{M} := \vec{B} - \frac{\gamma}{\gamma+1}\vec{\beta}\times\vec{E} \tag{2.16}$$

$$\vec{N} := \frac{\gamma}{\gamma+1}\left(\vec{E} + \vec{\beta}\times\vec{B}\right)\times\vec{\beta} \tag{2.17}$$

$$\vec{\tilde{M}} := \vec{E} + \frac{\gamma}{\gamma+1}\vec{\beta}\times\vec{B} \tag{2.18}$$

$$\vec{\tilde{N}} := \frac{\gamma}{\gamma+1}\left(-\vec{B} + \vec{\beta}\times\vec{E}\right)\times\vec{\beta} \tag{2.19}$$

$$\vec{R} := \vec{M} + \gamma \vec{N} \tag{2.20}$$

$$\vec{\tilde{R}} := \vec{\tilde{M}} + \gamma \vec{\tilde{N}}. \tag{2.21}$$

The spatial part of the four velocity is $\vec{\beta}$. The vector $\vec{N}$ can be rewritten as

$$\vec{N} = \frac{\gamma}{\gamma+1}\left(\vec{E}\times\vec{\beta} - \vec{\beta}\left(\vec{B}\cdot\vec{\beta}\right) + \vec{B}\vec{\beta}^2\right). \tag{2.22}$$

and $\vec{\tilde{N}}$ can also be written as

$$\vec{\tilde{N}} = \frac{\gamma}{\gamma+1}\left(-\vec{B}\times\vec{\beta} - \vec{\beta}\left(\vec{E}\cdot\vec{\beta}\right) + \vec{E}\vec{\beta}^2\right). \tag{2.23}$$

To simplify Equation 2.15 the terms inside the brackets can be redrafted:

$$\vec{\omega}_\mu = \frac{\mu}{I\gamma}\vec{R} - \frac{e}{m}\vec{N} = \frac{ge}{2Im\gamma}\vec{R} - \frac{e}{m}\vec{N} \tag{2.24}$$

$$\begin{aligned} &= \frac{e}{m}\frac{gs}{2I\gamma}\left(\vec{B} - \gamma/(\gamma+1)\vec{\beta}\times\vec{E} + \frac{\gamma^2}{\gamma+1}\left(\vec{E}\times\vec{\beta} - \vec{\beta}\left(\vec{B}\cdot\vec{\beta}\right) + \vec{B}\vec{\beta}^2\right)\right) - \\ &\qquad \frac{\gamma}{\gamma+1}\frac{e}{m}\left(\vec{E}\times\vec{\beta} - \vec{\beta}\left(\vec{B}\cdot\vec{\beta}\right) + \vec{B}\vec{\beta}^2\right) \end{aligned} \tag{2.25}$$

$$\begin{aligned} &= \frac{e}{m}\frac{gs}{2I\gamma}\left(\gamma\vec{B} + \gamma\vec{E}\times\vec{\beta} - \frac{\gamma^2}{\gamma+1}\vec{\beta}\left(\vec{B}\cdot\vec{\beta}\right)\right) - \\ &\qquad \frac{\gamma}{\gamma+1}\frac{e}{m}\left(\vec{E}\times\vec{\beta} - \vec{\beta}\left(\vec{B}\cdot\vec{\beta}\right) + \vec{B}\vec{\beta}^2\right). \end{aligned} \tag{2.26}$$

Using $I = 1$ and repeating the same calculation above for the EDM part yields [16]

$$\begin{aligned} \frac{d\vec{s}}{dt} = \frac{e}{m}\vec{s}\times&\left[\left(a+\frac{1}{\gamma}\right)\vec{B} - \frac{a\gamma}{\gamma+1}\vec{\beta}\left(\vec{\beta}\cdot\vec{B}\right) - \left(a+\frac{1}{\gamma+1}\right)\vec{\beta}\times\vec{E}\right] \\ &+\frac{e}{m}\vec{s}\times\left[\frac{\eta}{2}\left(\vec{E}+\vec{\beta}\times\vec{B} - \frac{\gamma}{\gamma+1}\vec{\beta}\left(\vec{\beta}\cdot\vec{E}\right)\right)\right], \end{aligned} \tag{2.27}$$

where

$$a = \frac{g-2}{2} \tag{2.28}$$

is the anomalous magnetic moment and g is the Landé factor.
Using Equation 2.14 and the condition $\vec{\beta}\cdot\vec{E} = \vec{\beta}\cdot\vec{B} = 0$ the observed spin motion [18]

is

$$\frac{d\vec{s}}{dt} = \frac{e}{m}\vec{s} \times \left[a\vec{B} - \left(a - \frac{1}{\gamma^2 - 1}\right)\vec{\beta} \times \vec{E} + \frac{\eta}{2}\left(\vec{E} + \vec{\beta} \times \vec{B}\right)\right]. \tag{2.29}$$

To include the gradient field to Equation 2.29 the term [16]

$$\frac{d\vec{s}}{dt} = \frac{\mu}{Im}\frac{1}{\gamma + 1}\vec{s} \times \left(\vec{\beta} \times \vec{\nabla}\right)\left[\vec{s} \cdot \vec{R}\right] + \frac{d}{Im}\frac{1}{\gamma + 1}\vec{s} \times \left(\vec{\beta} \times \vec{\nabla}\right)\left[\vec{s} \cdot \tilde{\vec{R}}\right] \tag{2.30}$$

must be added.

2.2.2 Influence of Gravitation

The description of the effect of gravitation on the spin motion requires the application of the theory of general relativity. The equation without the gradient fields [19] has the form

$$\frac{DS^i}{D\tau} = \frac{dS^i}{d\tau} + \Gamma^i_{kl}S^k u^l = \frac{q(1+a)}{2m}(F^i_k S^k + u^i F^{kl} S_k u_l) - u^i S_k \frac{Du^k}{D\tau} + \frac{q\eta}{2m}\epsilon^{iklm}F_{kj}S_l u^j u_m. \tag{2.31}$$

The Christoffelsymbol $\Gamma^\alpha_{\beta\gamma}$ is defined as

$$\Gamma^\alpha_{\beta\gamma} = \frac{g^{\alpha\mu}}{2}\left(\partial_\beta g_{\mu\gamma} + \partial_\beta g_{\mu\gamma} - \partial_\mu g_{\beta\gamma}\right) \tag{2.32}$$

where $g_{\alpha\beta}$ is the metric of the system and a solution to the Einstein equation [20]. The metric contains the information about the curvature of space and time.
Including the gradient field effects from Equation 2.11 the equation takes the form

$$\begin{aligned}\frac{DS^i}{D\tau} = \frac{dS^i}{d\tau} + \Gamma^i_{kl}S^k u^l = \frac{q(1+a)}{2m}(F^i_k S^k + u^i F^{kl} S_k u_l) - u^i S_k \frac{Du^k}{D\tau} + \frac{q\eta}{2m}\epsilon^{iklm}F_{kj}S_l u^j u_m + \\ \frac{\mu}{Im}u_\nu u_\mu S^\gamma D_\gamma \hat{F}^{\mu\sigma}S_\sigma + \frac{d}{Im}u_\nu u_\mu S^\gamma D_\gamma F^{\mu\sigma}S_\sigma.\end{aligned} \tag{2.33}$$

The covariant derivative in general relativity is connected with the curvature of space time by the Christoffelsymbols $\Gamma^\mu_{\nu\lambda}$. For a second rank tensor the covariant derivative D_μ has the form

$$D_\mu T^{\alpha\beta} = \partial_\mu T^{\alpha\beta} + \Gamma^\alpha_{\mu\nu}T^{\nu\beta} + \Gamma^\beta_{\mu\nu}T^{\alpha\nu}. \tag{2.34}$$

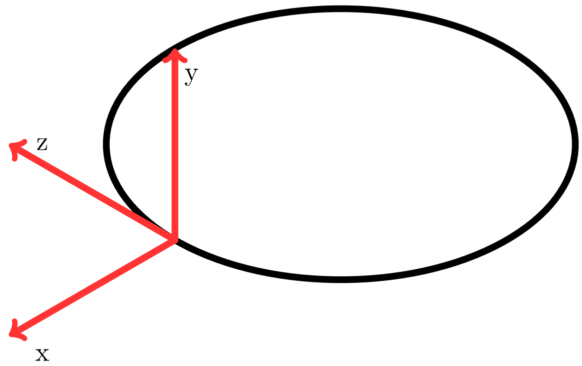

Figure 2.1: A comoving coordinate system where the black line symbolizes an arbitrary beam path in an accelerator.

Furthermore every form of energy is a source of a gravitational field. Thus electromagnetic fields and gravitation are a coupled system.
The equation of motion 2.11 of the beam can be transferred in the same way to a covariant form regarding the general theory of relativity. The effect of gravitation on the Frozen Spin concept is summarised in Chapter 3.3.4.

2.2.3 Comoving Coordinate System

For the description of the particle motion in the accelerator a comoving coordinate system is used (compare Figure 2.1). The radial direction is x, the vertical direction is y and z describes the coordinate along the tangential direction of beam line.

2.2.4 Spin Tune

The spin tune ν is defined as the number of spin rotations in the accelerator plane with respect to the number of particle cycles in the accelerator:

$$\nu = \frac{\omega_{s_{xz}}}{\omega_{\text{Cyclotron}}}, \tag{2.35}$$

where $\omega_{s_{xz}}$ is the angular frequency of spin rotation in the accelerator plane and $\omega_{\text{Cyclotron}}$ is the angular frequency of particle cycles. Otherwise, the vertical spin build up is similar defined by

$$\nu_{\text{V}} = \frac{\omega_{s_y}}{\omega_{Cyclotron}}, \tag{2.36}$$

where ω_{s_y} is the angular frequency of spin rotation in the vertical plane.

2.2.5 Spin Coherence Time

In a system of many particles the physical properties like the velocity differ. Thus the angular velocities of the spin rotations do not match the required Frozen Spin conditions and the polarisation of the beam in the plane of the accelerator decrease. The spin coherence time (SCT) is defined as the time difference between the start of the experiment and that point in time when the width of the spin distribution reaches 1 rad [21].
The average effect of the leading order contribution of the particle deviations in the radial and in the vertical direction is supressed by betatron oscillations [4]. To decrease further the momentum deviations of the beam two methods are applied. A RF cavity supresses the leading error. Furthermore sextupoles are used to vanish the effect of the next leading order [4], [22].
Experiments proved the possibility to inject a polarized beam and to keep a SCT of 1000 s using different families of sextupoles [23].

2.2.6 Period of Measurement

The total time of measurement t_{total} is determined by the desired statistical error. The following calculations for the statistical error determination are based on a note by J. Pretz [24].
The vertical build up of the polarisation is linear to the magnitude of the EDM (compare Section 3.1). Thus the build up can be described by

$$P_V = Pn\nu_{\text{V}}2\pi = Pn\eta\tilde{\nu}_V 2\pi \tag{2.37}$$

where n is the number of turns in the accelerator and $\nu_V = \eta \cdot \tilde{\nu}_{\text{V}}$ is the vertical spin tune. Thus the measured EDM is

$$\vec{d} = \frac{P_{\text{V}}}{P}\frac{\tilde{\nu}_{\text{V}}}{n}\frac{e}{2m}\vec{s}\frac{1}{2\pi}. \tag{2.38}$$

The error of the vertical polarisation is

$$\sigma_{P_{\text{V}}} = \frac{1}{\sqrt{NfAP}} \tag{2.39}$$

where N is the number of filled particles, f is the detection efficiency, A is the analysing power and P is the polarisation of the beam. Thus the statistical error of one fill is

$$\sigma_d = \left| \frac{\tilde{\nu}_{\mathrm{V}}}{n} \frac{es}{2m} \frac{1}{\sqrt{NfA}} \frac{1}{2\pi} \right| . \tag{2.40}$$

The value of n is defined by the revolution frequency f_{cycl} and the period of one run. This period is normally defined by the SCT τ. This results in

$$\sigma_d = \left| \frac{\tilde{\nu}_{\mathrm{V}}}{f_{\mathrm{cycl}}\tau} \frac{es}{2m} \frac{1}{\sqrt{NfA}} \frac{1}{2\pi} \right| . \tag{2.41}$$

The statistical error is proportional to $1/\sqrt{N_{\mathrm{fills}}}$ with the number of fills $N_{\mathrm{fills}} = \frac{t_{\mathrm{total}}}{\tau}$. This leads to

$$\sigma_d(t_{\mathrm{total}}) = \left| \frac{\tilde{\nu}_{\mathrm{V}}}{f_{\mathrm{cycl}}} \frac{es}{2m} \frac{1}{\sqrt{NfAP}} \frac{1}{\sqrt{t_{\mathrm{total}}\tau}} \frac{1}{2\pi} \right| . \tag{2.42}$$

Demanding a limit for the statistical error $\sigma_d(t_{\mathrm{total}})$ the total time of measurement can be estimated by

$$t_{\mathrm{total}} = \left(\left| \frac{\tilde{\nu}_{\mathrm{V}}}{f_{\mathrm{cycl}}} \frac{es}{2m} \frac{1}{\sqrt{NfAP}} \frac{1}{\sqrt{\tau}} \frac{1}{2\pi} \right| 1/\sigma_d(t_{\mathrm{total}}) \right)^2 . \tag{2.43}$$

The value for $\tilde{\nu}$ is determined in Chapter 5.1.3. Characteristic values for the quantities N, f, τ and A are listed in Table 2.2.

A	0.6 [25]
N	$4 \cdot 10^7$ [25]
f	$5 \cdot 10^{-3}$ [25]
τ	1000 s [23]

Table 2.2: Characteristic values of N, f, τ and A.

3 Applied Methods and Systematic Effects

This chapter presents the setup of the experiment. Furthermore the effect of different systematics on the measurement are discussed. Finally a method to eliminate these effects is presented.

3.1 Frozen Spin Ring

The Frozen Spin Ring concept was proposed by srEDM [4] and is summarised in this section. The basic idea is to use a storage ring and dispose the spin motion due to a magnetic momentum to measure the EDM of charged hadrons. The initial polarization is aligned parallel to the beam direction.
The EDM signal is the vertical build up of the polarization

$$\Delta P_V = P\frac{\omega_{\text{EDM}}}{\Omega}\sin(\Omega t + \theta_0) \tag{3.1}$$

where $\Omega = \sqrt{|\vec{\omega}_{\text{EDM}}|^2 + |\vec{\omega}_\mu|^2}$, $\vec{\omega}_{\text{EDM}}$ is the angular velocity of the spin rotation due to the EDM, $\vec{\omega}_\mu$ respectively the MDM, P is the polarization of the beam, t is the time and θ_0 the initial offset. The spin motion caused by the magnetic dipole moment would hide the effect of the EDM. Thus the part should fulfil

$$\vec{\omega}_\mu = \frac{q}{m}\left[\left(a\vec{B}\right) + \left(-a + \frac{1}{\gamma^2 - 1}\right)\vec{\beta}\times\vec{E}\right] \hat{=} 0 \tag{3.2}$$

by an appropriate choice of magnetic and electric fields in the accelerator. Thus $\theta_0 = 0$ and $\Omega \to 0$ assuming that $\omega_{\text{EDM}} \cdot t \ll 1$ the vertical spin build up can be approximated by

$$\Delta P_V \approx P\omega_{\text{EDM}}t.$$

Using the Lorentz force and the centrifugal force the cyclotron angular frequency $\vec{\omega}_{\text{Cyclotron}}$ for a deflector device can be determined by

$$\vec{\omega}_{\text{Cyclotron}} = \frac{q}{p}\left(\vec{\beta}\times\vec{B} + \vec{E}\right), \tag{3.3}$$

where p is the momentum of the reference particle. Furthermore, the electromagnetic fields emitted by the E×B deflectors have a non-vanishing radial electric field and a vertical magnetic field.

$$\vec{B} = (0, 0, B)^T, \quad \vec{E} = (E, 0, 0)^T, \quad \vec{v} = (0, \beta, 0)^T \tag{3.4}$$

$$\vec{\beta} \times \vec{E} = (0, 0, -\beta E)^T, \quad \vec{\beta} \times \vec{B} = (\beta B, 0, 0)^T \tag{3.5}$$

Using Equation 3.3 the elecric field is

$$E = \frac{\gamma m \beta^2}{qr} - \beta B. \tag{3.6}$$

Using the Condition 3.2 E and B can be determined by

$$0 = aB - \left(\frac{1}{\gamma^2 - 1} - a\right) \beta E \tag{3.7}$$

$$B = E\beta/a \left(\frac{1}{\gamma^2 - 1} - a\right) \tag{3.8}$$

$$E = \frac{\gamma m \beta^2}{qr} \cdot \frac{1}{\left(\frac{1}{\gamma^2-1} - a\right) \beta^2/a + 1} \tag{3.9}$$

$$\Rightarrow B = \frac{\gamma m \beta^2}{qr} \cdot \frac{\left(\frac{1}{\gamma^2-1} - a\right)}{\left(\frac{1}{\gamma^2-1} - a\right) \beta^2/a + 1} \frac{\beta}{a}. \tag{3.10}$$

One possibility to avoid misleading errors caused by magnetic fields is to construct a storage ring with pure electro static elements [11]. The disadvantage of this concept is that the EDM of particles with $a < 0$ cannot be measured. The reason is that for a pure electro static ring the Frozen Spin condition is $\left(\frac{1}{\gamma^2-1} - a\right) \beta E = 0$. The condition $a < 0$ implies that $\frac{1}{\gamma^2-1} < 0$. The value of γ is by definition larger or equal to one. Thus it is not possible to fulfil the Frozen spin condition using E fields and a magic momentum [11]. The anomalous magnetic momenta of some particles are listed in the next paragraph.

3.1.1 Suitable Particles for the Frozen Spin Experiment

The choice of deuterons for this experiment has several reasons. The isospin behaviour of the EDM is unknown [10]. Thus the EDM of neutrons, protons and other particles must be measured. So far no direct measurement of the deuteron EDM exists.

The anomalous magnetic moment is defined by Equation 2.28

$$a = \frac{g-2}{2}. \tag{3.11}$$

A small anomalous magnetic moment a minimises the spin rotation caused by the magnetic fields [4]. The most suited particles would have $a = 0$ which is impossible. Leptons with $a = \mathcal{O}(0.001)$ [4] would be the best solution but electrons are heavily effected by synchrotron radiation. Moreover muons or tauons are not stable [26] and have a small flux due to the production processes.
The Landé factor g of the deuteron is $g = \frac{m_D}{m_p} \cdot 0.857\,438\,231\,1(48)$ [27] with $m_p = 938.272\,046(21)\,\mathrm{MeV}$ [26] and the mass of deuterons is $m_D = 1875.612\,859(41)\,\mathrm{MeV}$ [26]. The resulting anomalous magnetic moment is

$$a = -0.142\,987\,27(38).$$

An overview of anomalous magnetic momenta for different light particles are listed in Table 3.1. Hence the proton contains a small a compared to protons or ^{3}HE.

Particle	Leptons	Protons	Deuterons	^{3}HE
a	~ 0.001 [4]	$1.792\,847(1)$ [10]	$-0.142\,987\,27(38)$ [27],[26]	$-4.183\,963(1)$ [10]

Table 3.1: Anomalous magnetic momentum for different particles.

Regarding the previous Section the EDM measurement of protons with $a > 0$ is possible via a pure electrostatic ring. However, deuterons require the use of electric and magnetic fields.

3.1.2 Properties of Frozen Spin Lattice

A possible lattice design [5], [28] is shown in Figure 3.1a. The corresponding optical functions are plotted in Figure 3.1b. The beam properties of the simulations are enlisted in Table 3.2. The whole lattice is implented in the extension of COSY Toolbox [29].

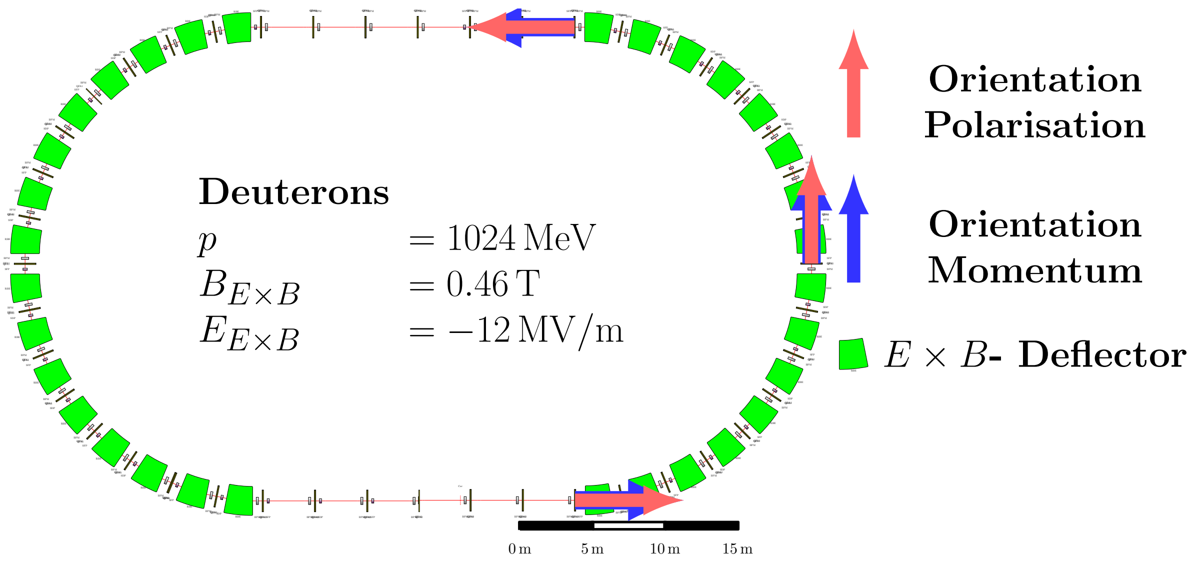

(a) The lattice of the simulated Frozen Spin ring.

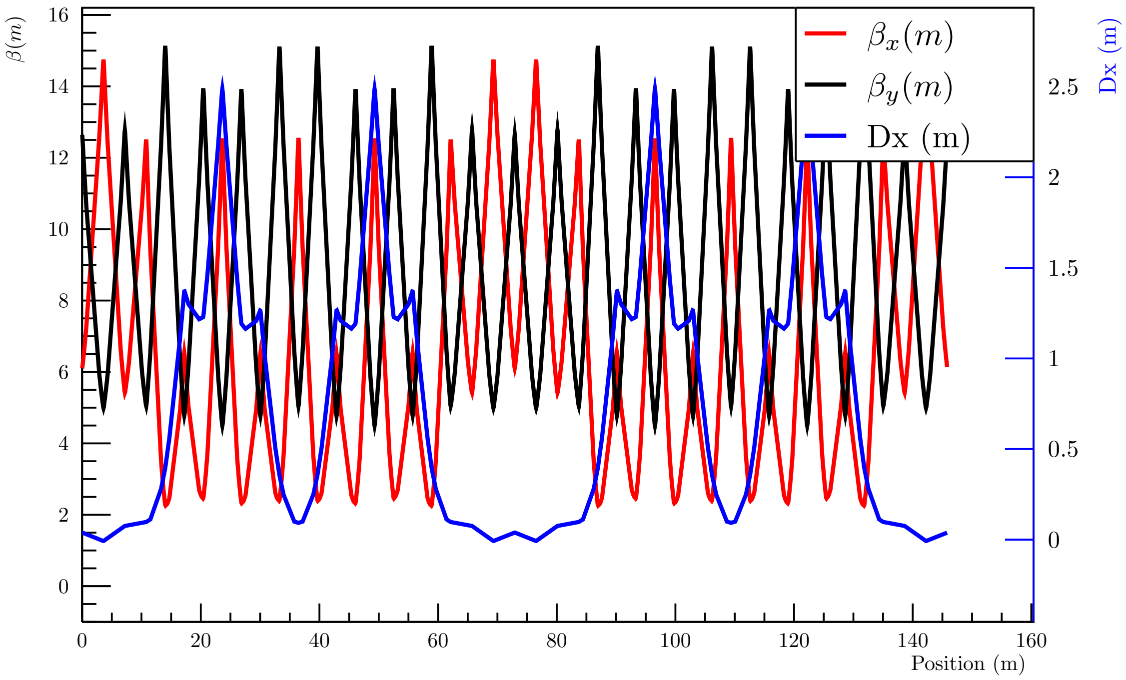

(b) The optical functions of the simulated Frozen Spin ring.

Figure 3.1: The simulated Frozen Spin ring lattice.

γ	1.144 02
β	0.485 726
B	0.46 T
E	−12 MV/m
m	1875.61 MeV $\hat{=}$ 3.343 58 · 10^{-27} kg
a	−0.142 987
r_0	9.206 249 74 m
p	1024 MeV
Total length	145.845 m
Time per turn	≈ 9.9721 · 10^{-7} s

Table 3.2: Properties of the beam in the simulated Frozen Spin ring.

3.2 Quasi Frozen Spin Ring

A similar concept to the Frozen Spin is the Quasi Frozen Spin Ring [30],[5]. A corresponding lattice design [5] is presented in Figure 3.2b. One complicated technical issue of the Frozen Spin concept is the construction of the curved E×B deflectors. To avoid this task the idea is to use standard magnetic deflectors to curve the beam and use straight curved E×B deflectors to steer the horizontal polarization. Figure 3.2b displays the motion of the horizontal polarization in the accelerator. At the entrance of one arch the orientation of the horizontal polarization is tangential to the momentum direction. The spin tune ν in a pure magnetic field can be described by

$$\nu = \frac{\omega_{\text{spin}}}{\omega_{\text{Cyclotron}}} = \frac{q/maB_V}{qB_V/(\gamma m)} = \gamma a. \tag{3.12}$$

Hence the spin is rotated by $\gamma a \pi$ after one arch. The following straight deflectors compensate this rotation in such way that at the beginning of the next arch the horizontal polarization is again aligned parallelly with the direction of the beam motion.
The setup of the electric and magnetic fields are calculated in [5]. To include subleading effects as well, the following calculation will cover fringe fields as well. The polarization in the magnetic deflectors is rotated by $\Theta_0 = \nu \frac{L_0}{2\pi \langle r_0 \rangle} 2\pi = \nu \frac{L_0}{\langle r_0 \rangle}$ where L_0 is the length of the deflector and $\langle r_0 \rangle$ is the effective bending radius of this deflector. The z dependent magnetic and electric field can be described by $B(z) = Bf_1(z)$ and $E(z) = Ef_2(z)$ where E and B are the amplitudes. This implies

$$\Theta_0 = \gamma a L_0 \left\langle \frac{1}{r} \right\rangle. \tag{3.13}$$

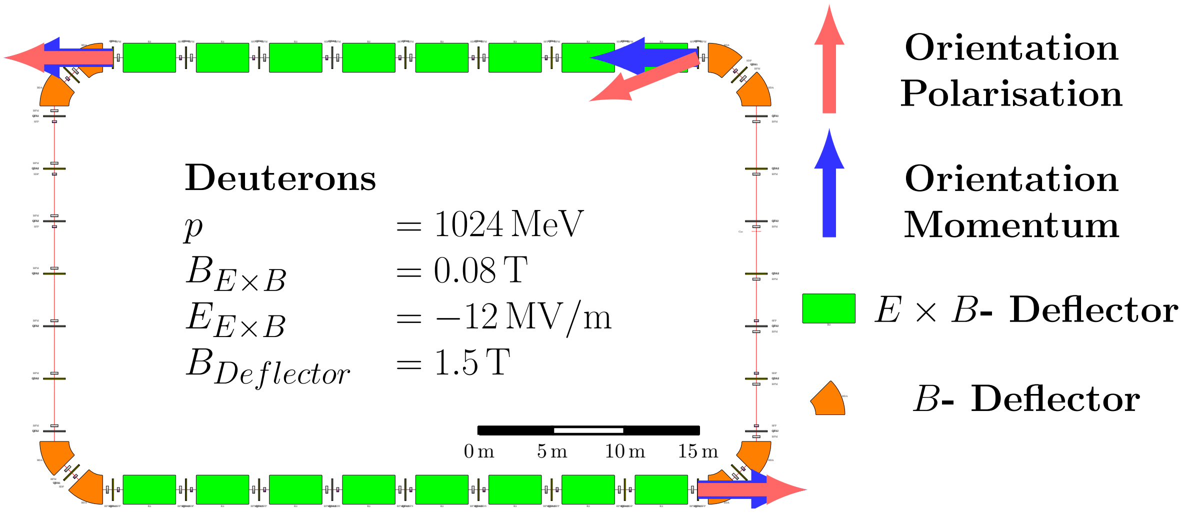

(a) Quasi Frozen Spin Ring Lattice.

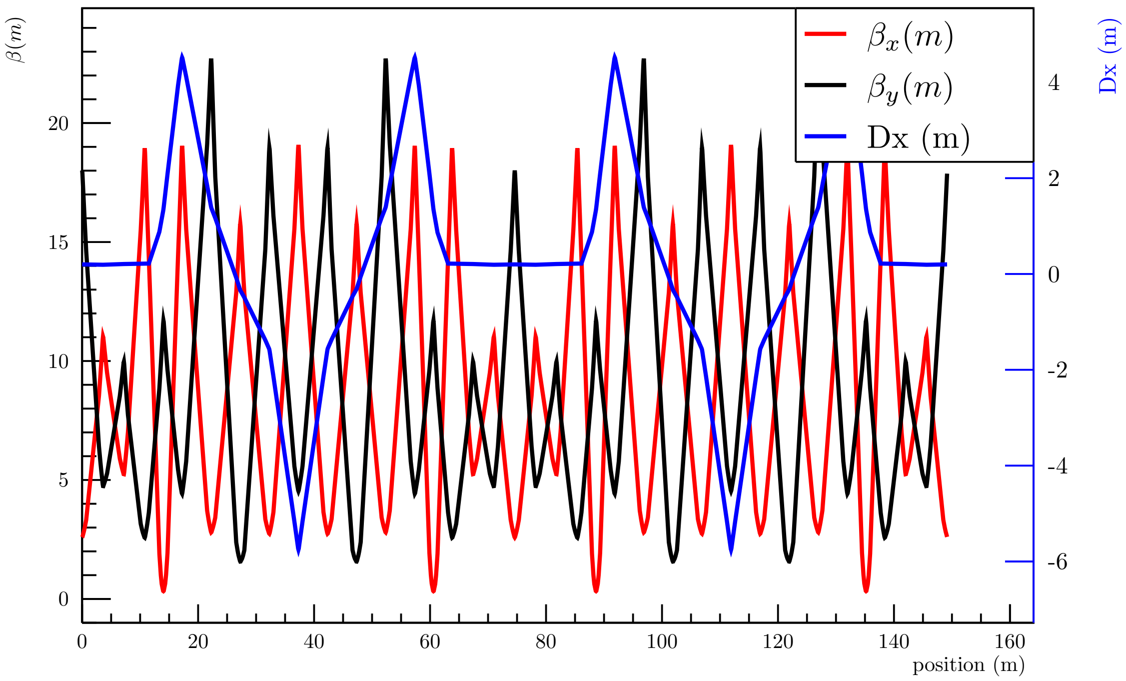

(b) Quasi Frozen Spin Ring optical functions.

Figure 3.2: The simulated Quasi Frozen ring lattice and the corresponding optical functions.

The Lorentz force inside the E×B deflectors is zero.

$$0 = q\beta B \int_{z_0}^{z_1} f_1(s)ds + qE \int_{z_0}^{z_1} f_2(s)ds \;\Rightarrow E = -B\beta \int_{z_0}^{z_1} f_1(s)ds \Big/ \int_{z_0}^{z_1} f_2(s)ds \tag{3.14}$$

The deflection angle is determined by

$$\Theta = 1/\beta \int_{z_0}^{z_1} \left(aBf_1(s) - \left(\frac{1}{\gamma^2 - 1} - a \right) \beta E f_2(s) \right) ds \tag{3.15}$$

$$\begin{aligned} \Theta = \frac{q}{m\beta} \int_{z_0}^{z_1} \Bigg(& aBf_1(s) \\ & + \left(\frac{1}{\gamma^2 - 1} - a \right) \beta \left(B\beta \int_{z_0}^{z_1} f_1(s')ds' \Big/ \int_{z_0}^{z_1} f_2(s'')ds'' \right) f_2(s) \Bigg) ds \end{aligned} \tag{3.16}$$

$$\Leftrightarrow \Theta = \frac{Bq}{m\beta} \int_{z_0}^{z_1} f_1(s)ds \left(a + \left(\frac{1}{\gamma^2 - 1} - a \right) \beta^2 \right) \tag{3.17}$$

$$\Leftrightarrow \Theta = \frac{Bq}{m\beta\gamma^2} \int_{z_0}^{z_1} f_1(s)ds \, (a + 1) \tag{3.18}$$

The resulting fields are:

$$B = -\gamma^3 \frac{a}{a+1} L_0 \left\langle \frac{1}{r} \right\rangle \frac{m\beta}{q} / \int_{z_0}^{z_1} f_1(s)ds \tag{3.19}$$

$$E = \gamma^3 \frac{a}{a+1} L_0 \left\langle \frac{1}{r} \right\rangle \frac{m\beta^2}{q} / \int_{z_0}^{z_1} f_2(s)ds. \tag{3.20}$$

For vanishing fringe fields the same result as in [5] can be achieved:

$$B = -\Theta_0 \frac{\gamma^2}{a+1} m \frac{\beta^2}{q}, \; E = -\frac{B}{\beta}.$$

3.2.1 Properties of Simulated Quasi Frozen Spin Lattice

The beam properties for the simulated Quasi Frozen Spin lattice are enlisted in Table 3.3.

γ	1.144 02
β	0.485 726
B	0.082 453 6 T
E	−12.0066 MV/m
B_{Bend}	1.5 T
m	$1875.61\,\mathrm{MeV} \mathrel{\hat{=}} 3.343\,58 \cdot 10^{-27}\,\mathrm{kg}$
a	−0.142 987
r_0	$\approx 2.3\,\mathrm{m}$
p	1042.24 MeV
Total length	149.211 m
Time per turn	$\approx 1.0247 \cdot 10^{-6}\,\mathrm{s}$

Table 3.3: Properties of the beam in the simulated Quasi Frozen Spin ring.

3.3 Sources of Artificial Vertical Spin Build Up

The main task of developing the final EDM storage ring is to avoid systematics. In this chapter an analysis of possible systematics is presented:

- Vertical electric fields
- Transverse magnetic fields
- Longitudinal fields
- Gradient fields
- Gravitation

3.3.1 Transverse Magnetic and Vertical Electric Fields

Regarding $\vec{\omega}_\mu$ (Equation 3.2) transverse magnetic and vertical electrical fields could evoke an unwanted vertical spin build up.

Misalignments

One source of these undesired fields are misalignments of deflectors. Figure 3.3 shows the coordinate system inside a curved E×B deflector. E.g. transverse magnetic and a vertical electrical fields appear in the accelerator, if E×B deflectors are rotated around the longitudinal z axis.

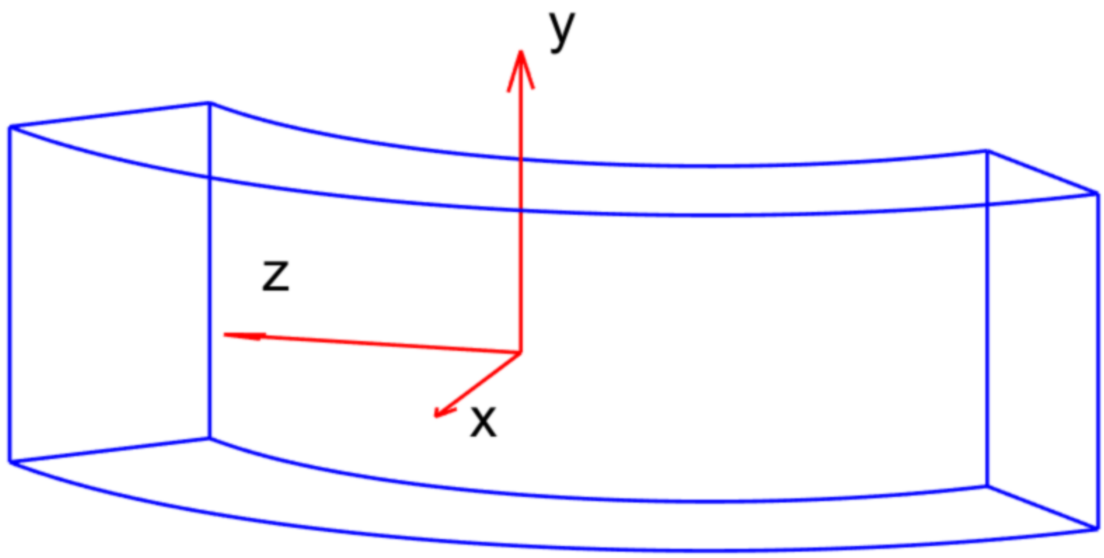

Figure 3.3: Representation of the used coordinate system inside an E×B deflector.

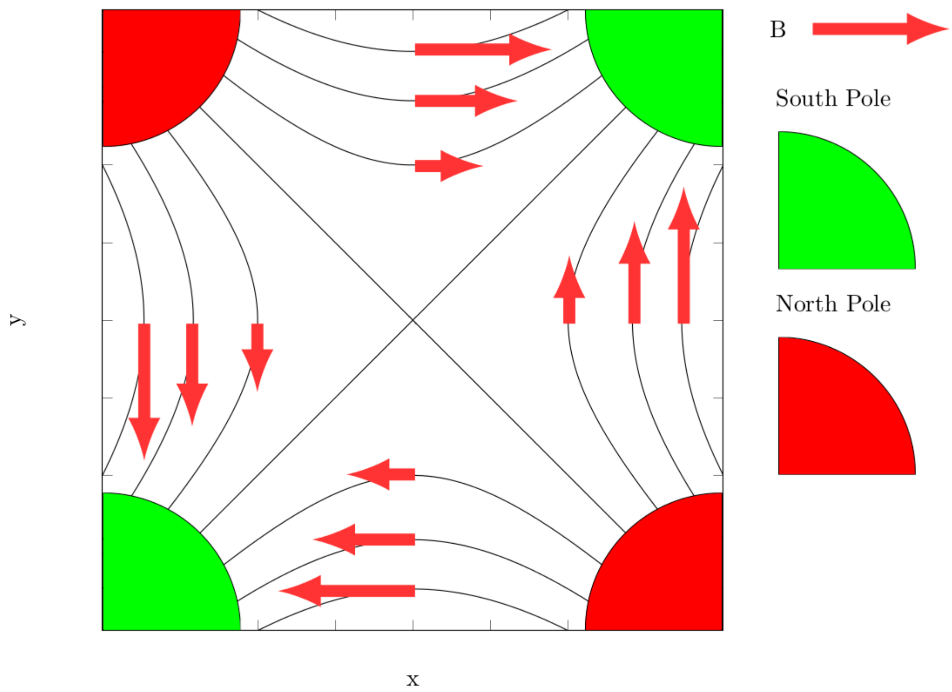

Figure 3.4: Magnetic field inside a quadrupole. At the center of the quadrupole the magnetic field vanishes.

Multipoles

The magnetic field of multipole magnets with more than two poles includes transverse magnetic fields by construction. The quadrupole magnetic fields can be described by

$$B_x = k \cdot x, B_y = k \cdot y. \tag{3.21}$$

where k is the gradient of the magnetic field. The magnetic fields of a quadrupole are plotted in Figure 3.4. In regard to the vertical beam emittance shifts in the vertical direction should evoke an additional vertical polarization build up. That is why the beam width in vertical direction has to be minimised.

3.3.2 Gradient Effect

Only homogeneous electromagnetic fields are considered in the Frozen and Quasi Frozen Spin concept. However, storage rings contain inhomogeneous fields. For example magnetic multipoles, which are necessary for beam correction. The inhomogeneous fields of a quadrupole are plotted in Figure 3.4.
Metodiev [16] proved that the effect of gradient fields vanishes in the Frozen Spin concept for the reference particles due the Frozen Spin conditions. One condition of the Frozen Spin concept is that the polarization in the lattice plane is always parallel aligned with the beam motion. This condition is not fulfilled for particles in phase space any more. However, in the Quasi Frozen Spin concept this condition is also broken for the reference particle. The maximum of the desired deflection for the reference particle in the simulated Quasi Frozen Ring lattice is $\gamma a \pi$ and therefore an effect due to gradient fields is expected.
The effect of these gradient fields cannot be treated within the framework of COSY INFINITY up to today. To estimate the magnitude of the effect of this gradient fields a simulation was performed.
Assuming that the particle does not deviate from the reference path, one cycle without the gradient field effect and one cycle including the gradient field effect inside quadrupoles are simulated for the Quasi Frozen Spin concept.
Hence, the spin motion inside a quadrupole can be determined. Using Equation 2.30 and neglecting the part of the EDM results in

$$\left(\frac{d\vec{s}}{dt}\right)_{\nabla} = \frac{\mu}{Im}\frac{1}{\gamma+1}\left(\vec{s}\times\left(\vec{\beta}\times\vec{\nabla}\right)\right)\left[\vec{s}\cdot\vec{R}\right] \tag{3.22}$$

with

$$\vec{R} = \gamma \vec{B} - \gamma \vec{\beta} \times \vec{E} - \frac{\gamma^2}{\gamma + 1} \left(\vec{\beta} \cdot \vec{B} \right) \vec{B}. \tag{3.23}$$

No electric fields and longitudinal magnetic fields are inside the quadrupoles:

$$\Rightarrow \vec{E} = 0, \vec{\beta} \cdot \vec{B} = 0 \Rightarrow \vec{R} = \gamma \vec{B}. \tag{3.24}$$

Applying the definition

$$\alpha' := \frac{\gamma}{\gamma + 1} \frac{\mu}{Im}, \tag{3.25}$$

the equation for the spin motion can be rewritten as:

$$\vec{s} \times \left(\vec{\beta} \times \vec{\nabla} \right) = \left[\vec{s} \cdot \vec{\nabla} \right] \vec{\beta} - \left[\vec{s} \cdot \vec{\beta} \right] \vec{\nabla} \tag{3.26}$$

$$\Rightarrow \left(\frac{d\vec{s}}{dt} \right)_{\nabla} = \alpha' \left(\left[\vec{s} \cdot \vec{\nabla} \right] \vec{\beta} - \left[\vec{s} \cdot \vec{\beta} \right] \vec{\nabla} \right) \vec{s} \cdot \vec{B} \tag{3.27}$$

$$\tag{3.28}$$

The spin is defined as

$$\vec{s} := \begin{pmatrix} s_x \\ s_z \\ s_y \end{pmatrix}. \tag{3.29}$$

The magnetic field inside the quadrupoles is

$$\vec{B} = \begin{pmatrix} k \cdot y \\ 0 \\ k \cdot x \end{pmatrix}. \tag{3.30}$$

Finally the spin motion inside a quadrupole for the Quasi Frozen lattice is

$$\left(\frac{d\vec{s}}{dt} \right)_{\nabla} = \alpha' \beta k \begin{pmatrix} -s_y s_z \\ 2 s_x s_y \\ -s_x s_z \end{pmatrix}. \tag{3.31}$$

Hence there should be a vertical spin build up for the reference particle inside quadrupoles. The simulations were done for different magnitudes of a possible deuteron EDM. MATLAB [31] and the corresponding ODE suite [32] were used for the simulations. The results are shown in Figure 3.5.

In addition the effect has the following proportionality

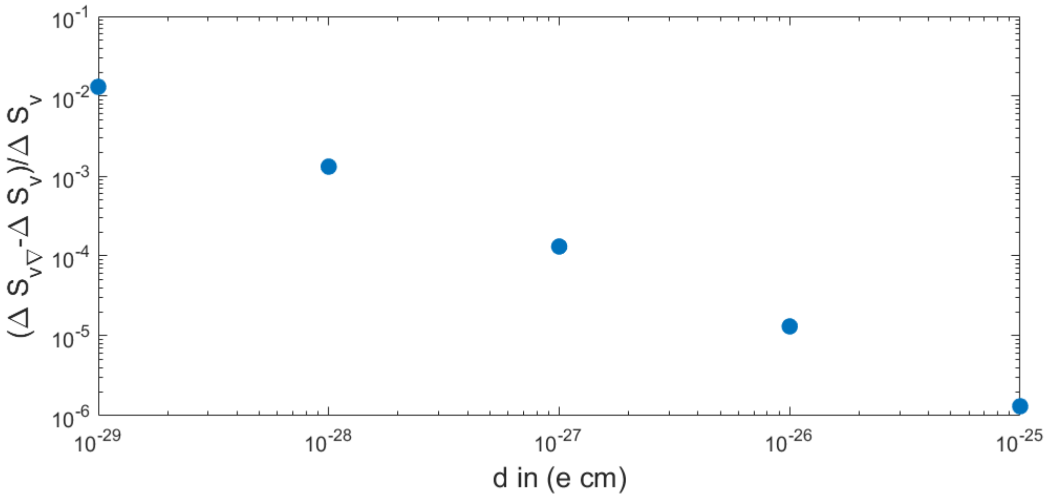

Figure 3.5: The relative difference for the vertical spin build up with an existing or respectively vanishing gradient field effect inside the quadrupoles.

$$\left(\frac{d\vec{s}}{dt}\right)_{\nabla} \propto \frac{\mu}{m} \propto \frac{g}{2m^2} \propto \frac{a+1}{m^2}. \tag{3.32}$$

Thus the gradient effect is negligible for much heavier particles than deuterons. Moreover, the deflection of the polarization is proportional to a and the gradient effect depends on the radial components of the spin. Hence it could be expected that the gradient field effect of protons is at least 2 magnitudes larger than for the deuterons.

A remark regarding leptons, the effect would be more than 6 magnitudes larger in the Quasi Frozen concept and non reference particles would also generate large systematics in the Frozen Spin concept.

All in all for EDMs $\gg 10^{-29}$ e cm the effect can be neglected for deuterons. But for the final EDM measurement where the prediction by SM for the magnitude of EDM of deuterons is 10^{-29} e cm [4] a far more detailed simulation is necessary. If a measurement of the EDM of protons in the same ring is desired, the gradient field effect potentially exceeds the observable spin build up and therefore masks the EDM.

3.3.3 Longitudinal Magnetic and Electric Fields

For the computation of the Frozen and Quasi Frozen Spin conditions longitudinal fields are neglected. Unfortunately longitudinal fields cannot be disregarded. Longitudinal magnetic fields appear by rotations of the E×B and magnetic deflectors around the x axis. Longitudinal electric fields can occur by rotations around the vertical axis.
Considering only longitudinal fields the effect of longitudinal fields can be estimated

$$\vec{B} = \begin{pmatrix} 0 \\ B \\ 0 \end{pmatrix}, \vec{E} = \begin{pmatrix} 0 \\ E \\ 0 \end{pmatrix}. \tag{3.33}$$

Neglecting the EDM part of Equation 2.27

$$\frac{d\vec{s}}{dt} = \frac{e}{m}\vec{s} \times \left[\left(a + \frac{1}{\gamma}\right)\vec{B} - \frac{a\gamma}{\gamma+1}\vec{\beta}\left(\vec{\beta}\cdot\vec{B}\right) - \left(a + \frac{1}{\gamma+1}\right)\vec{\beta}\times\vec{E}\right] = \tag{3.34}$$

$$\frac{e}{m}\left[\left(a + \frac{1}{\gamma}\right)\begin{pmatrix} -s_y \cdot B \\ 0 \\ s_x \cdot B \end{pmatrix} - \frac{a\gamma}{\gamma+1}(\beta \cdot B)\begin{pmatrix} -s_y \cdot \beta \\ 0 \\ s_x \cdot \beta \end{pmatrix}\right] \tag{3.35}$$

the effect of longitudinal fields can be analysed.
Referring to the Equation 3.35, longitudinal electrical fields do not effect the spin motion. However, longitudinal magnetic fields create a vertical spin build up if the spin is rotated and not aligned parallel with the momentum. If the spin is frozen ($s_x = 0$) and the vertical build up can be neglected and therefore the right hand side of Equation 3.35 vanishes.
Hence it should be expected that longitudinal magnetic fields only yield a negligible contribution to the Frozen Spin concept compared to the Quasi Frozen Spin concept. Regarding Section the maximum deflection angle of the reference particle is $\gamma a \pi$ in the Quasi Frozen Spin lattice.

3.3.4 Gravitation

The pure gravitational effect on the spin in a Frozen Spin ring is estimated by Orlov et al. [19] using Equation 2.31

$$\left(\frac{ds_{\mathrm{V}}}{dt}\right)_{\mathrm{Grav}} \approx \frac{g}{\beta}s_z \tag{3.36}$$

where g is the acceleration of gravity. Thus the influence of gravitation on the spin would cause vertical polarization build of

$$\left(\frac{ds_{\mathrm{V}}}{dt}\right)_{\mathrm{Grav}} \approx s_z \cdot 7 \cdot 10^{-8}\,1/\mathrm{s} \tag{3.37}$$

using $\beta \approx 0.59$ and $g = 9.81\,\mathrm{m\,s^{-2}}$. For the final EDM ring with a desired precision of $\sigma_d = 10^{-29}\,\mathrm{ecm}$ the magnitude of the vertical build up caused by the EDM would be

$$\mathcal{O}\left(\left(\frac{ds_{\mathrm{V}}}{dt}\right)_{\mathrm{EDM}}\right) = s_z \cdot 10^{-8}\,1/\mathrm{s}. \tag{3.38}$$

Thus the gravitation would hide the EDM signal, if this systematic effect is not corrected. Orlov et al. [19] suggests to correct this systematics by the use of Equation 3.36. Another method is presented in the next section

3.3.5 Spin Invariant Axis

The spin invariant axis of a ring is defined as the axis where no spin motion is observed if the spin is parallel aligned to this axis after one turn. The vertical axis is the spin invariant axis in the simulated lattices, if no EDM exists. The spin motion caused by the the EDM and the spin invariant axis have to be in one plane otherwise additional misleading spin motions occur [33]. An effect of a tilt of the spin invariant axis by the EDM is the reduction of the spin build up [33].

3.4 Clockwise Counterclockwise Method

The different systematics avoid a measurement of the EDM. A solution to this problem is suggested by srEDM. They proposed a way to avoid the systematics by vertical electrical fields called the clockwise counterclockwise (CW-CCW) method [4]. The basic principle is to inject one beam after another in the opposite direction. The srEDM prefers to use a pure electrostatic ring for the EDM measurement of protons. In regard to the Lorentz force the direction of the electrical field does not change. For the E×B deflectors this is still true and the magnetic deflectors must change their setting for both injection directions.

Replacing the kinematics to obtain the counterclockwise beam

$$\vec{\beta} \to -\vec{\beta} \tag{3.39}$$

$$\vec{s}_{\text{Initial}} \to -\vec{s}_{\text{Initial}} \tag{3.40}$$

$$\vec{E} \to \vec{E} \tag{3.41}$$

$$\vec{B} \to -\vec{B} \tag{3.42}$$

the spin motion behaves differently for both injection directions. The injected spin direction is $\vec{s}_{\text{Initial}}$. The equation for the spin motion Equation 2.15 is

$$\frac{d\vec{s}}{dt} = \vec{s} \times (\vec{\omega}_\mu + \vec{\omega}_{\text{EDM}}) = \vec{s} \times \left[\underbrace{\frac{\mu}{I\gamma}\vec{R} - \frac{e}{m}\vec{N}}_{\vec{\omega}_\mu} + \underbrace{\frac{d}{I\gamma}\vec{\tilde{R}}}_{\vec{\omega}_{\text{EDM}}} \right]. \tag{3.43}$$

The components behaves under the applied changes as follows

$$\vec{R}_{\text{CCW}} = -\gamma\vec{B} + \gamma\vec{\beta} \times \vec{E} - \frac{\gamma^2}{\gamma+1}\left(\vec{\beta} \cdot \vec{B}\right)\vec{\beta} = -\vec{R}_{\text{CW}} \tag{3.44}$$

$$\vec{\tilde{R}}_{\text{CCW}} = \vec{E} - \frac{\gamma}{\gamma+1}\vec{\beta} \times \vec{B} + \frac{\gamma}{\gamma+1}\left(\vec{B} - \vec{\beta} \times \vec{E}\right) \times \vec{\beta} = \vec{\tilde{R}}_{\text{CW}} \tag{3.45}$$

$$\vec{N}_{\text{CCW}} = -\vec{N}_{\text{CW}} \tag{3.46}$$

The indices CW and CCW symbolizes clockwise or counterclockwise. The injection direction dependent behaviour can be used to build the difference of the vertical spin tune to extract the EDM and to erase unwanted effects by disturbing transverse or longitudinal fields.

3.4.1 Counterclockwise Method Gradient Fields

Taking gradient fields into account, the equation for the gradient field effect is Equation 3.22

$$\left(\frac{d\vec{s}}{dt}\right)_{\nabla} = \vec{s} \times \underbrace{\frac{\mu}{Im}\frac{1}{\gamma+1}\left(\vec{\beta} \times \vec{\nabla}\right)[\vec{s} \cdot \vec{R}]}_{\vec{\omega}_{\nabla}}. \tag{3.47}$$

Applying the condition of the inversed beam

$$\vec{\omega}_{\nabla CCW} = \frac{\mu}{Im}\frac{1}{\gamma+1}\left(-\vec{\beta}\times\vec{\nabla}\right)\left[-\vec{s}\cdot\left(-\vec{R}_{CCW}\right)\right] = -\vec{\omega}_{\nabla CW} \tag{3.48}$$

it can be proven that the gradient field effect has the same behaviour as the MDM for the CCW beam.

3.4.2 Counterclockwise Method Gravitation

At last the effect of CW-CCW is discussed for the gravitational effect. For the clockwise beam is the vertical spin motion

$$\left(\frac{ds_{\mathrm{V}}}{dt}\right)_{\mathrm{Grav}} \approx \frac{g}{\beta}s_z. \tag{3.49}$$

Using the substitutions from Section 3.4 to translate to the CCW configuration

$$\left(\left(\frac{ds_{\mathrm{V}}}{dt}\right)_{\mathrm{Grav}}\right)_{\mathrm{CCW}} = \frac{g}{-\beta}\left(-s_z\right) = \left(\left(\frac{ds_{\mathrm{V}}}{dt}\right)_{\mathrm{Grav}}\right)_{\mathrm{CW}}. \tag{3.50}$$

Therefore the angular velocity $\vec{\omega}_{Grav}$ for the gravitational effect has the same behaviour as for the MDM, too.

3.4.3 Counterclockwise Method Overview

Table 3.4 summarises the behaviour of the effect of CW-CCW on the discussed effects. All in all the presented systematics has an opposite spin build regarding the CW-CCW method than the EDM.

Effect	CW	CCW
EDM	$+$	$+$
MDM	$+$	$-$
Gradient field	$+$	$-$
Gravitation	$+$	$-$

Table 3.4: Sign of angular velocity $\vec{\omega}$ of spin rotation $\frac{d\vec{s}}{dt} = \vec{s}\times\vec{\omega}$ due to different effects. The $'+'$ for the CW method characterises the original direction of $\vec{\omega}$. A $'+'$ of the CCW method represents the same direction of $\vec{\omega}$ for the reversed beam motion and a $'-'$ characterises the opposite motion of $\vec{\omega}$.

4 Utilized Simulation Programs and Software Extensions

This chapter presents the used simulation software. Moreover, extensions of the utilized framework are discussed.

4.1 COSY INFINITY

Spin tracking and lattice design can be done by using the program COSY INFINITY. COSY INFINITY uses differential algebraic techniques to calculate taylored transfer maps in arbitrary computing accuracy [6]. It is written in Fortran77. COSY INFINITY uses its own script language.
For particle tracking transfer maps are used. These transfer maps have the benefits to enable fast simulations. This paragraph presents the basics of transer maps and is based on the first chapter of the book *Modern Map Methods in Particle Beam Physics* [34].
A transfer map is a function which describes the development of space points. If a state of space points can be described by $\vec{x}_1$ at the time t_1 then the space points $\vec{x}_2$ at t_2 are described by the transfer map via

$$\vec{x}_2 = M_{t_1,t_2}(\vec{x}_1) \tag{4.1}$$

if the system is deterministic. For the case of repetition the space points transformation between arbitrary points in time via

$$M_{t,\Delta t} = M_{t+\Delta t, t+2\Delta}. \tag{4.2}$$

The consequence is that only one transformation map $M_{t,\Delta t}$ must be calculated for the simulation. The space points at different times are determined by the repetitive application of this map. This ability of transfer maps enables fast particle or spin tracking compared to integration methods [35].

4.2 COSY Toolbox

COSY Toolbox (COTOBO) is an existing C++ based interface [7] for COSY INFINITY 9.1 and ROOT [36]. For this thesis ROOT 6 [37] is used. COTOBO was developed for spin tracking simulations for the COSY accelerator in Jülich. Moreover the management of many different simulations is simplified by the utilisation of C++ and at last the usability of ROOT enables fast and easy way to analyse the simulation results. However, a full compatibility between both programs does not exists. For example some accelerator elements are not implemented in COSY Toolbox because it was developed in regard to the analysis of the COSY synchrotron. Thus necessary tools for the simulation of EDM storage rings are missing and must be added. Hence, the E×B deflectors are an example for not implemented elements. Furthermore the Quasi Frozen Spin concept contains sector magnets which must be included, too.

4.3 Modifications to COSY Toolbox

In this section some changes of COSY Toolbox are discussed. The list of adjustment contains only an extract of the main modifications and therefore it is incomplete. The compatibility with older COSY Toolbox versions is not tested. Some header files including further details are in the manual [29]. Moreover, an example of code to setup a spin tracking simulation including the new modifications is in the manual.

4.3.1 E×B Deflectors

COSY Toolbox was not designed for the simulation of E × B deflectors [38]. These elements are the basis of the Frozen Spin concept. Consequently these elements have to be added. COSY INFINITY contains two elements to simulate E×B deflectors which are called Wien Filters. The standard element in COSY INFINITY **WF** is a E×B deflector containing homogeneous magnetic and electric fields. The required input parameters are the bending radii according to the electric (r_E) and magnetic field (r_B), the length of the device and the aperture. The effective bending radius of the device is calculated via the Lorentz force

$$\vec{F}_L = q\vec{\beta} \times \vec{B} + q\vec{E} = \gamma m\vec{\omega} \times (\vec{\omega} \times \vec{r})\,. \tag{4.3}$$

Consider only a vertical magnetic field B_y, a radial electric field E_r and a velocity tangential to the reference path. Using these input parameters, the effective radius r_0

can determined by

$$q\beta B_z + qE_x = \gamma m \frac{\beta^2}{r_0} \tag{4.4}$$

$$\underbrace{\frac{qB_z}{\gamma m \beta}}_{1/r_B} + \underbrace{\frac{qE_x}{\gamma m \beta^2}}_{1/r_E} = \frac{1}{r_0}. \tag{4.5}$$

The corresponding implementation for COSY Toolbox is stored in *Wien.h* and *Wien.cc*. The user has to set up the electric and magnetic radii via *SetRadiusB(double)* or *SetRadiusE(double)*. The length and aperture are set up using the methods of the parent class *Element* function *SetLength(double)* and *SetAperture(double)*. The methods *SetB(double)* and *SetE(double)* can be used to save the desired values of the magnetic and electric fields but those values will not have any effect on the simulations.

Despite the simulation of E×B deflectors containing homogeneous fields, an element with the possibility to simulate multipoles exists. The corresponding element is called **WC** in COSY INFINITY. The element **WC** approximates the form of magnetic and electric fields via

$$F(x) = F_0 \left[1 + \sum_{i=1}^{n} N_i x^i \right]$$

where n defines the highest order of simulated multipoles and N_i are the coefficients for the electric or magnetic field. The electric in radial direction and the magnetic field in vertical direction respectively is $F(x)$. Thus the dependency of the magnetic field can only be described in one direction apart from fringe fields (compare 4.3.2).

In COSY Toolbox are the corresponding files *WienMultipole.h* and *WienMultipole.cc*. The methods are the same as for the class *Wien* except that *WienMultipole* include methods to set up the coefficients. The magnetic coefficients can be set up via *SetMultipoleB(vector<double>)* and the electric per *SetMultipoleE(vector<double>)*. The maximum order of multipoles is set up via *SetNumMultipole(double)*.

The implementation of E×B deflectors is realised such that the simulation of fringe fields and misalignments is possible. The implementation for the misalignments simulation was realised in a similar way as the implementation for the magnetic deflectors.

In COSY Toolbox generated plots of the ring lattices of the E×B deflectors are represented by green elements. As an example the Quasi Frozen Ring lattice is depicted in Figure 4.1.

However, COSY INFINITY has not the necessary resources to generate a transfer map

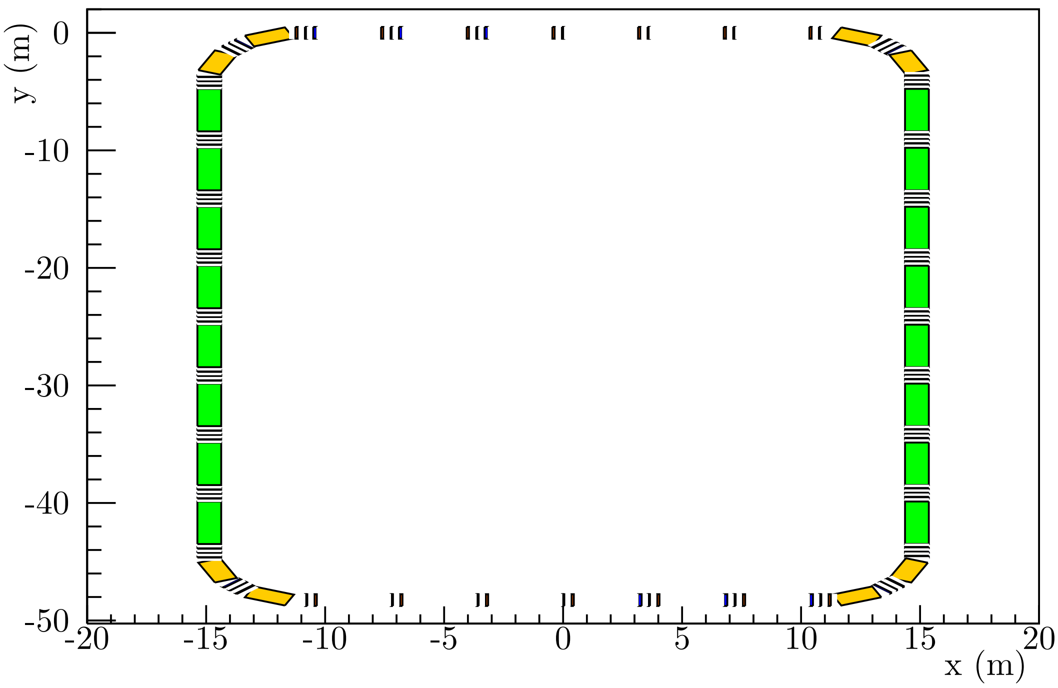

Figure 4.1: The generated lattice plot of COTOBO for the Quasi Frozen Ring lattice.

representing a E×B deflector including any desired magnetic or electric field component for a freely selectable point inside the deflector. These requirements are necessary to enable the analysis of the influence of construction errors and precision of the curved deflectors. Hence, for further spin tracking simulations integration algorithms are needed to analyse this point in the future.

4.3.2 Fringe Fields

To determine the shape of fringe fields simulations are needed. Electric fringe fields of capacitors can be described by implicit mapping [39], [40]. COSY INFINITY approximates the fringe [6] by

$$F(z) = \frac{1}{1 + \exp\left(\sum_{n=0}^{5} A_n \cdot [z/(2d)]^n\right)} \tag{4.6}$$

where A_n are coefficients, z is the coordinate on the beam line where the origin is the effective edge of the element, d is the aperture and $2d$ is the full aperture. The effective length of one element is defined by

$$l_{Eff} = \frac{1}{B_{max}} \cdot \int_{-\infty}^{\infty} B(z)dz, \tag{4.7}$$

where B_{max} is the amplitude of the magnetic field. The effective length of the electric field is defined in the same way. An example plot containing the effective length and device length is in Figure 4.2a.
In COSY Toolbox new coefficients for the simulation of electric fringe fields are introduced (compare Table 4.1). The class *Enge* manages the enge coefficients. These coefficients were determined by Eremey Valetov [41]. The updated shape of the fringe

Coefficient	Value
A_0	1.066717916109775
A_1	1.6215939887044952
A_2	-0.9713991696899339
A_3	0.466860288912587
A_4	-0.11809443899423651
A_5	0.011332163947410089

Table 4.1: Fringe field coefficients for electric fields [41].

functions are plotted in Figure 4.2b.

COSY INFINITY includes only coefficients for devices with a large length compared to the aperture size. The minimum required fraction is approximately $12 \cdot d$. Otherwise the fringe fields are not correctly simulated. For short elements the result is that the adjusted amplitude of the magnetic or electric field is not reached at the centre of the element, but could be much smaller than expected. Thus the ability to activate seperately the fringe fields for each simulated device is included. To adjust this option use *SetFlagFringeOff(true)* to deactivate the simulation of fringe fields of selected elements. Furthermore these elements contain a flag for the activated mode for the fringe field simulations. This is usually 3 [6] and can be passed by *SetFringeMode(fModeFringe)*.

4.3.3 Calculator for Ring Properties

To enable the setup of Frozen Spin and Quasi Frozen Spin lattices with different kinetic energies, particles, number of E × B deflectors tools are included to determine the magnetic and electric fields for both kind of rings.

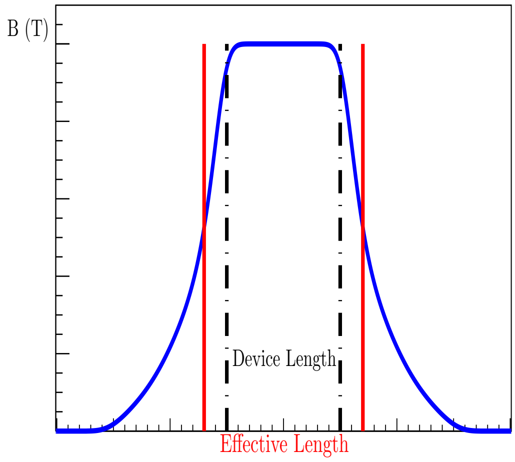

(a) Effective length of the magnetic field.

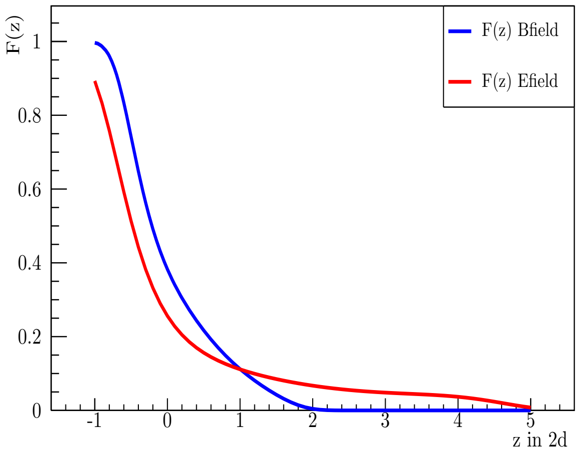

(b) Fringe field shape.

Figure 4.2: Shape of fringe fields and the device length compared with the effective length.

Thus the class *RelPart* is included to determine the relativistic quantities of one particle. The input of the class is the energy and mass of the particle. All relativistic quantities of the particle can be extracted in SI and natural units.
The virtual base class *SpinRing* offers methods to set up the ring properties (i.e. particle type or radius). In addition the functions *vector<double> GetB()*, *vector<double> GetE()*, *vector<double> GetREffB()* and *vector<double> GetREffE()* to extract the desired values for the electromagnetic fields and effective radii are included.
The child classes *FrozenSpinRing* and *QuasiFrozenWienRing* include the method *void Calculate()* to determine the desired values.

4.3.4 Spin Analysis

Another class is developed to analyse the spin motion and the spin rotation in the vertical direction and in the plane of the accelerator. The following section bases on a contribution to the annual report of the Forschungszentrum Jülich [42].
The class *Tracker* of COTOBO can be used to store the particle and spin tracking results for an arbitrary step size and number of particles.
The class *SCTimeCalculator* extracts this data from the corresponding ROOT files. The usage of *Quicksort* [43] within the parent class *SCTime* leads to an efficient sorting procedure to the final analyse of the extracted data. For sorting efficiently, *SCTime*. *SCTime* contains methods to calculate the development of the spin motion and the spin

spread.
Two main quantities can be determined: the spin tune ν and the spin coherence time τ_{SCT}. For the spin tune the mean polarization orientation in the horizontal plane of the simulated beam for each turn is calculated. For the Frozen Spin condition a linear change of the orientation θ with respect to the beam direction is assumed. The angle depends on the turn number n:

$$\theta(n) = \theta_0 + 2\pi\nu \cdot n. \tag{4.8}$$

The initial deflection angle is θ_0. The description of the spread σ of the distribution of the polarization orientation in the horizontal plane is similar:

$$\sigma(t) = \sigma_0 + \alpha \cdot t \tag{4.9}$$

The initial polarization spread is σ_0 and the maximum acceptable spread is $\sigma_{SCT} = 1\,\mathrm{rad}$. Hence SCT can be calculated by

$$\tau_{SCT} = \frac{\sigma_{SCT} - \sigma_0}{\alpha}. \tag{4.10}$$

4.3.5 List of Ring Elements

To check the properties of the installed ring the *Calculator* method *Save()* automatically generates a ROOT object of *TNamed RingElements*. This object contains a list of all elements including the name, length, aperture, electric fields, magnetic fields and information about the multipole components.

4.3.6 Sector and Rectangular Bending Magnets

COSY Toolbox includes only rectangular magnets. The simulated Quasi Frozen Spin lattice uses sector magnets to avoid further misleading effects due to the non perpendicular fringe fields of the rectangular magnets with respect to the motion of the particles. The class *MagneticBend* [38] has the new flag *bool fIsSectorMagnet* to choose between sector and rectangular magnets. The default value is *true* and activates the simulation for sector magnets. When the flag is changed to *false* rectangular magnets are simulated.

4.4 Ring Lattices

The lattices of both rings are implemented in different classes. The Frozen Ring lattice are implemented in *FrozenRingRef1* and *FrozenRingRef1Fringe*. The corresponding classes for the Quasi Frozen Ring lattices are *QFrozenRingRef1* and *QFrozenRingRef1Fringe*. For both rings default settings are initialised via the constructors. The elements and properties of a simulated ring object can be changed at will.
A spin tracking simulation via COSY Toolbox requires an object of *ElementList* including all elements of the lattice [38] . The corresponding method is *GetEList()*.
To simulate a CCW beam the method *Reverse()* reverses the order of the elements in the lattice and set up the physical properties of the elements for a CCW beam.

5 Simulation Results

This chapter lists the simulation results and determination of the spin tune. In addition the time of measurement is estimated by using the spin tune. Afterwards the influence of misalignments are simulated. Each time at first for the Frozen Spin and then for the Quasi Frozen Spin lattice the misalignment results are presented. Finally the simulation results for the CW-CCW method are presented.

5.1 Spin Tune

In the final ring a CW and CCW beam are simulated. In both simulations the polarization points towards the beam motion. The CW and CCW behaviour of the simulation set up is tested for single particles containing the same phase-space configuration. For these particles the spin motion behaviour is confirmed. For the final simulations the polarization is determined for a bunch of particles. Due to the limited number of particles, which is between 1000 and 10000, and slight deviations of the spin invariant axis small deviations for CW-CCW method can occur. The values of the simulated emittances and momentum deviation are listed in Table 5.1.

ϵ_x	1 mm mrad
ϵ_y	1 mm mrad
$\frac{\Delta p}{p}$	10^{-4}

Table 5.1: Magnitudes of simulated emittances.

This section presents the determination of $\tilde{\nu}$ for the Frozen and Quasi Frozen lattice. This quantity is necessary to determine the final time of measurement and to validate the CW-CCW method.

5.1.1 Frozen Spin

Figure 5.1a displays the vertical polarization build up due to the EDM for the CW and CCW beam for different fringe field models. One time the hard edge model without fringe fields is simulated and the second time the fringe field is simulated, too. As expected the build-up changes the direction dependent on the beam direction. The difference between the vertical build up for CW and CCW is plotted in Figure 5.1b. The value for the vertical spin tune $\tilde{\nu} = \nu/\eta$ times 2π is extracted and is used for the analysis of the

CW-CCW method for the the correction of misalignments. The relationship between η and d of deuterons is

$$\eta \approx d \cdot 1.9 \cdot 10^{14}\,\mathrm{e\ cm}^{-1},\ d \approx \eta \cdot 5.3 \cdot 10^{-15}\,\mathrm{e\,cm} \tag{5.1}$$

(compare Section 2.1.1). The simulated range is $\eta = 10^{-10}...10^{-7}$. The results for the both fringe field simulations is nearly the same. The determined value is $2\pi\tilde{\nu} \simeq 2.127$.

5.1.2 Quasi Frozen Spin

The simulated Quasi Frozen spin lattice contains nearly the same properties for the CW-CCW beam for the EDM (Figure 5.2a) and the vertical polarization build up (Figure 5.2b) as for the Frozen ring lattice with $2\pi\tilde{\nu} \simeq 2.104$. Thus commutativity due to the rotation of the polarization in different directions is not a misleading effect in a perfect Quasi Frozen ring. The relative difference for the calculated results of $2\pi\tilde{\nu}$ of both lattices is nearly 1%.

5.1.3 Statistical Error

Regarding Section 2.2.6 the time of measurement is described by Equation 2.43.

$$t_{\text{total}} = \left(\left| \frac{\tilde{\nu}_V}{f_{\text{cycl}}} \frac{es}{2m} \frac{1}{\sqrt{NfAP}} \frac{1}{\sqrt{\tau}} \frac{1}{2\pi} \right| 1/\sigma_d(t_{\text{total}}) \right)^2 . \tag{5.2}$$

Inserting all values from Section 2.2.6, $P \approx 1$, $f_{\text{cycl}} \approx 10^6$ and $2\pi\tilde{\nu}_V \approx 2.1$ and a desired $\sigma_d = 10^{-29}\,\mathrm{e\,cm}$ this results in a measurement time of about $1.1 \cdot 10^7\,\mathrm{s}$ what is less than one year. However, it can be confirmed that the statistical error is not an obstacle for the EDM measurement.

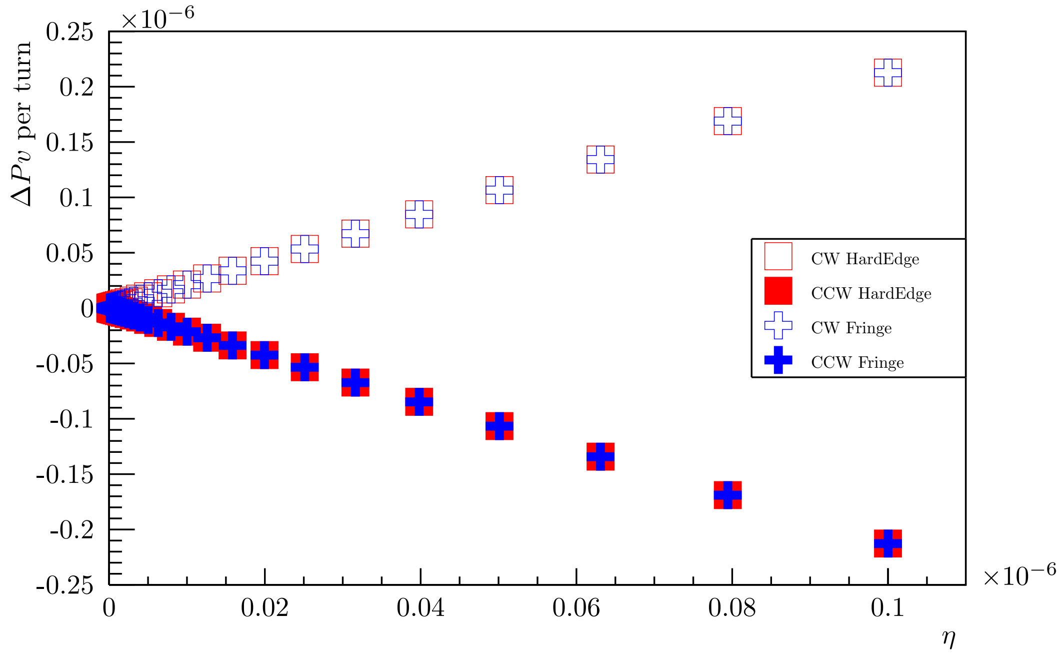

(a) Frozen Spin - Vertical spin build up per turn with respect to the magnitude of EDM for CW and CCW injected beams.

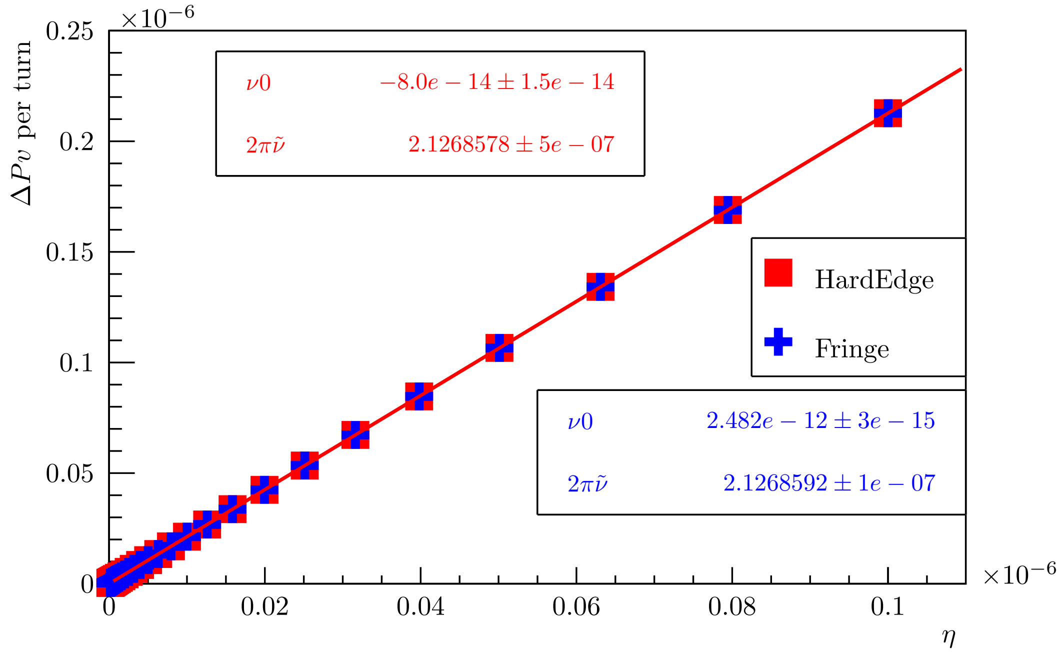

(b) Frozen Spin - Determination of the vertical spin tune $\tilde{\nu}$ depending on η. The plot contains the difference of the vertical polarization build up of the CW-CCW (Figure 5.1a) beam divided by 2.

Figure 5.1: Vertical spin build up for the simulated Frozen Spin lattice.

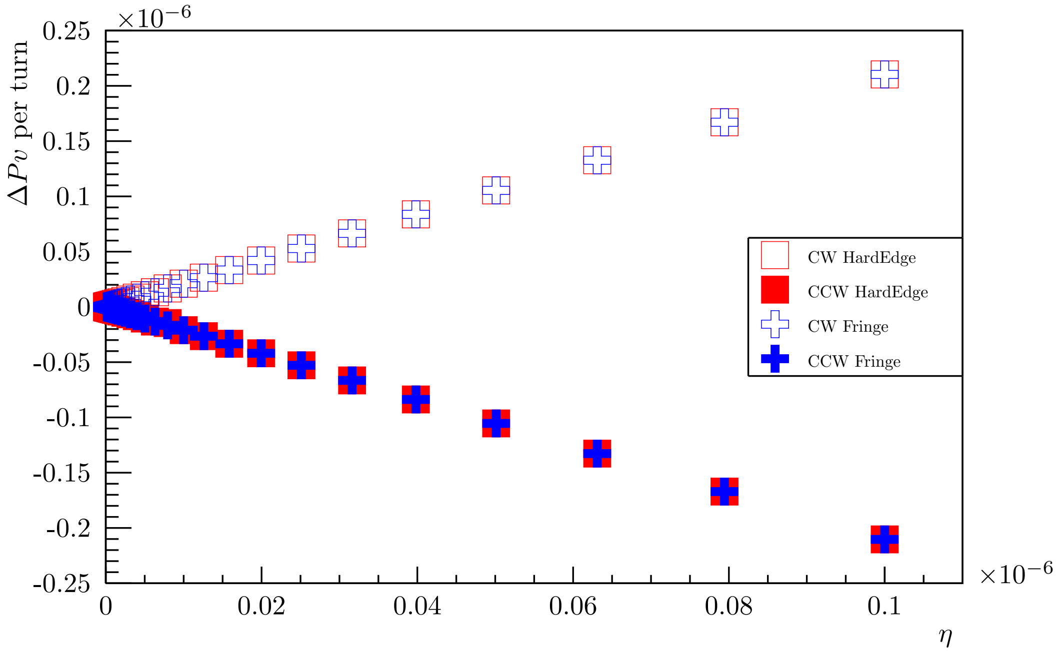

(a) Quasi Frozen Spin - Vertical spin build up per turn with respect to the magnitude of EDM for CW and CCW injected beams.

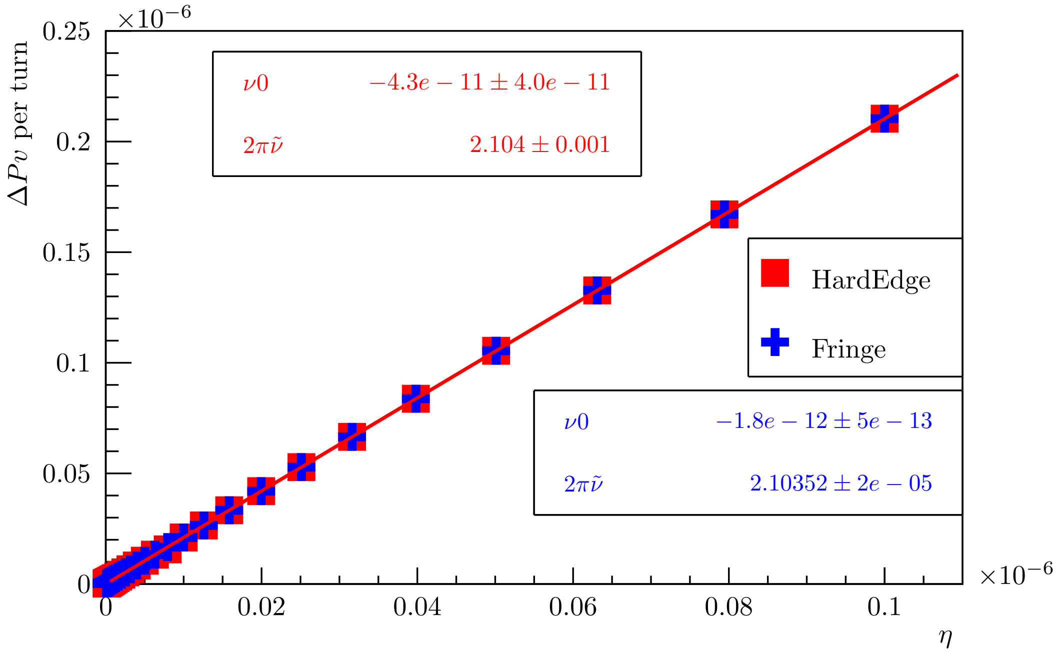

(b) Quasi Frozen Spin - Relative difference for vertical spin build up per turn with respect to the magnitude of EDM for CW and CCW injected beams.

Figure 5.2: Vertical spin build up for the simulated Quasi Frozen Spin lattice.

5.2 Simulation of Misalignments

To examine the effect of different misalignments of the devices on the spin behaviour the misalignments are randomly generated using a Gaussian distribution. Two cases are simulated. At first different misalignments like misalignment of the quadrupoles are simulated. For this case a large range of root mean square (RMS) of different misalignments of the devices in the accelerators are generated and the vertical polarization build up is simulated. Each simulation contains another set of randomly generated misalignments to determine the influence of each misalignment on the vertical spin build up.
The second set of simulations checks the CW-CCW method for a set of misalignments. For all simulations the initial polarization is aligned parallel to the beam direction. The number of simulated turns is 10^4 and 10^3 particles are simulated.

5.2.1 Misalignments of Deflectors

Rotations around Vertical Axis

Rotations around the vertical axis of the E×B deflectors result in longitudinal electric fields which should have no effect on the polarization regarding Section 3.3.3. The corresponding simulations are shown in Figure 5.3a for the Frozen Spin Concept. No influence of this misalignments on the vertical polarization motion is observed. The Quasi Frozen Spin concept has the same result (Figure 5.3b).

Rotations around Longitudinal Axis

Rotations of E×B deflectors around the longitudinal axis results in vertical electric fields and radial magnetic fields. This results in an artificial vertical polarization build up (compare Section 3.3.1).
Regarding Figure 5.4a is the rotation around the longitudinal axis the largest misleading effect in the Frozen Spin due to rotations of deflectors. This plot shows that for RMS smaller than 10^{-7} rad an EDM with $\eta = 10^{-7}$ is not influenced. Hence, a measurement of an existing EDM with $\eta = 10^{-7}$ is possible for such a small RMS value. For larger RMS values the misalignments create an artifical spin build up which prohibits an EDM determination. For smaller values of ηs and even a non existing EDM an artificial EDM signal is measured due to this misalignments. Thus, this large uncorrected effect would prevent the measurement of the EDM.
In the Quasi Frozen Ring concept the rotations of deflectors around the longitudinal

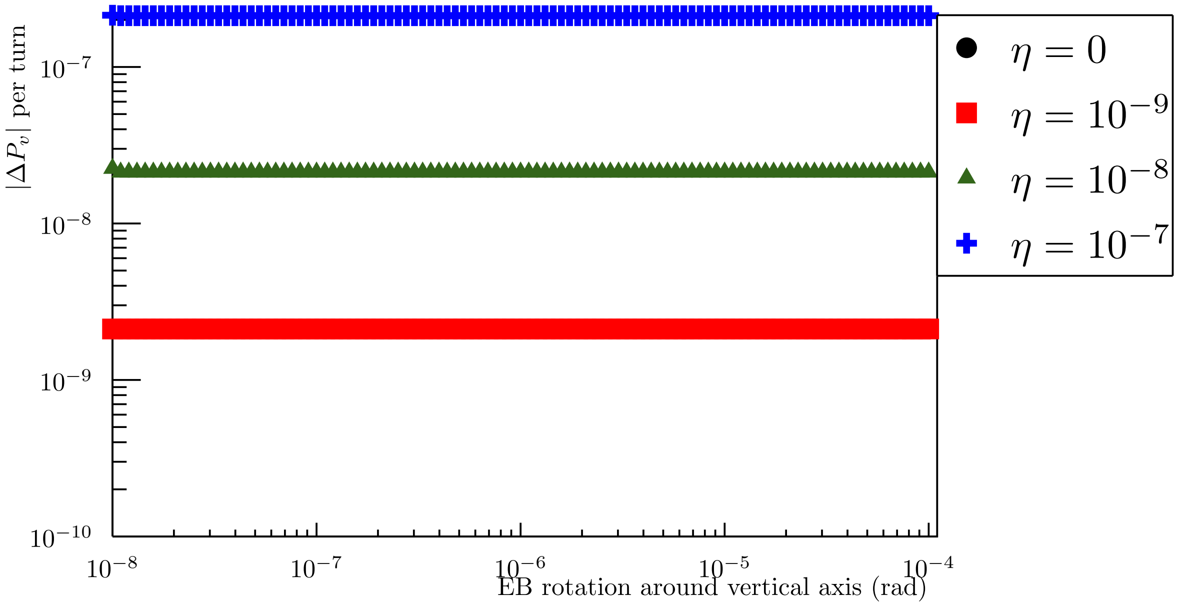

(a) Frozen Spin simulation.

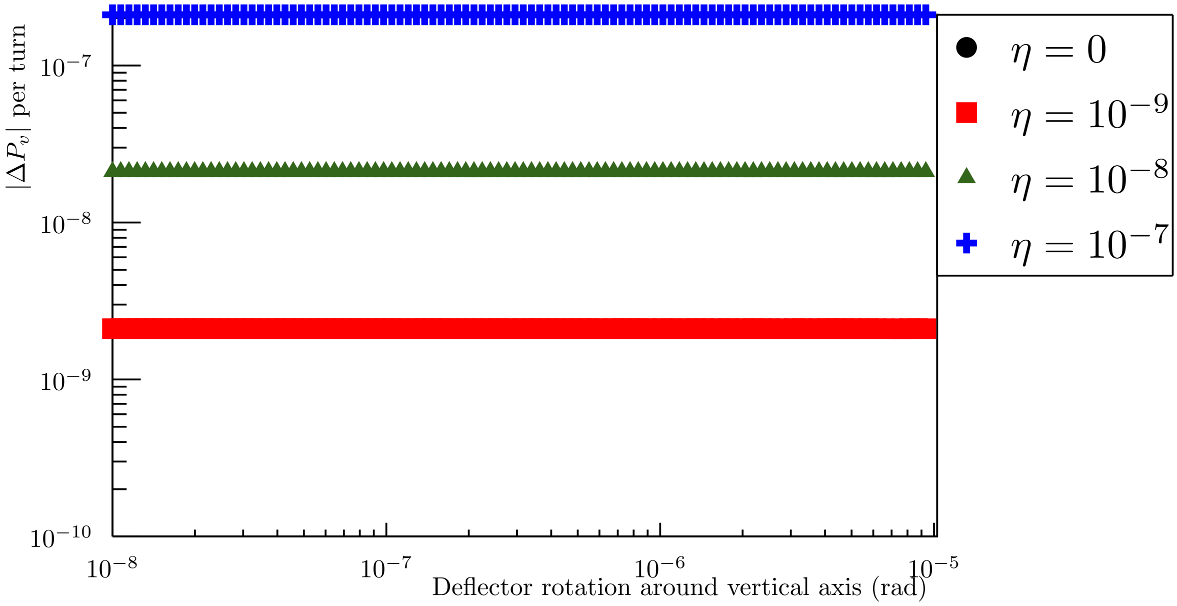

(b) Quasi Frozen Spin simulation.

Figure 5.3: Vertical spin build up for different magnitudes of EDM and RMS of rotation misalignments of the deflectors around the vertical axis. Each simulation has new randomly generated misalignments.

axis have the same magnitude as in the Frozen spin concept. In Figure 5.4b the results are shown.

Rotations around Radial Axis

Rotations around the radial axis of the E×B deflectors result in longitudinal magnetic fields which can influence the vertical polarization regarding section 3.3.3. The simulation results are plotted in Figure 5.5a. For small misalignment the curves for different EDM are saturated. For an increasing magnitude of misalignments the EDM signal is hidden and can not be measured without correction methods.
Opposite to the Frozen Spin concept rotations around the radial axis of the deflectors have a large influence in the Quasi Frozen Spin concept. This can be explained by the rotation of the polarization in the horizontal plane due to the pure magnetic deflectors (Section 3.3.3). The corresponding results are visualised in Figure 5.5b. The effect is even larger as the effect by rotations around the longitudinal axis for the Quasi Frozen Spin concept.

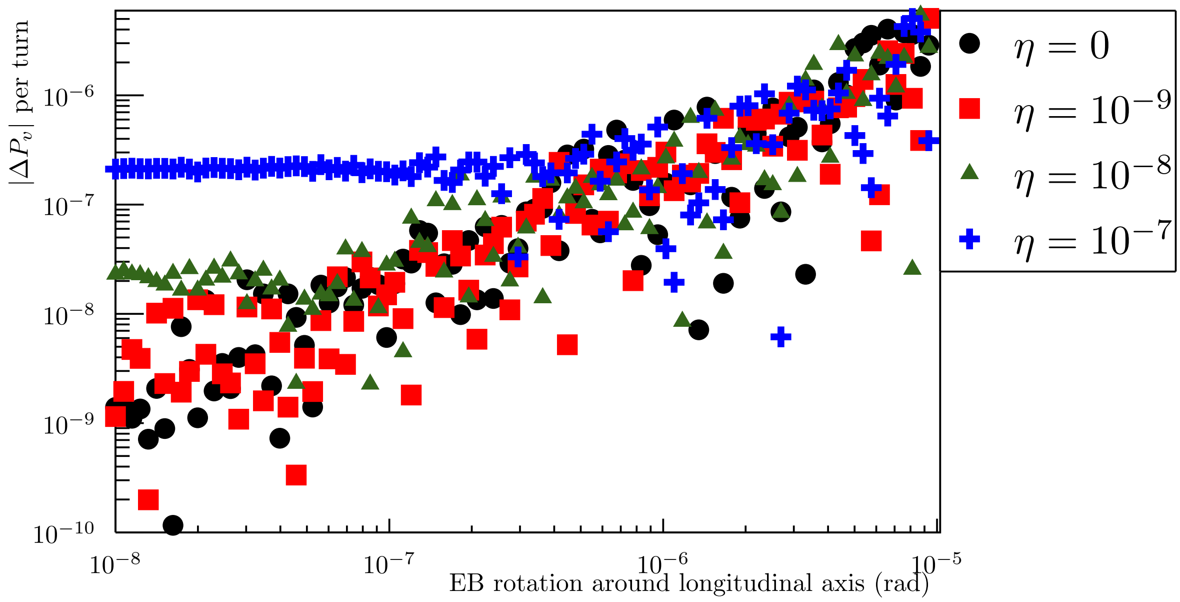

(a) Frozen Spin simulation.

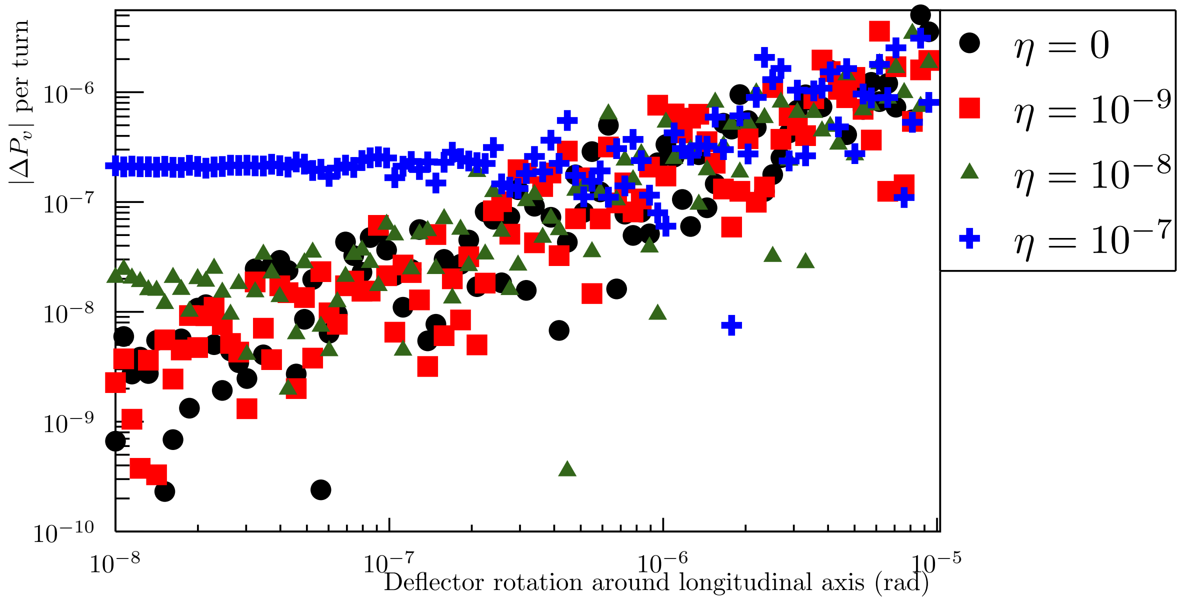

(b) Quasi Frozen Spin simulation.

Figure 5.4: Vertical spin build up for different magnitudes of EDM and RMS of rotation misalignments of the deflectors around the longitudinal axis. Each simulation has new randomly generated misalignments.

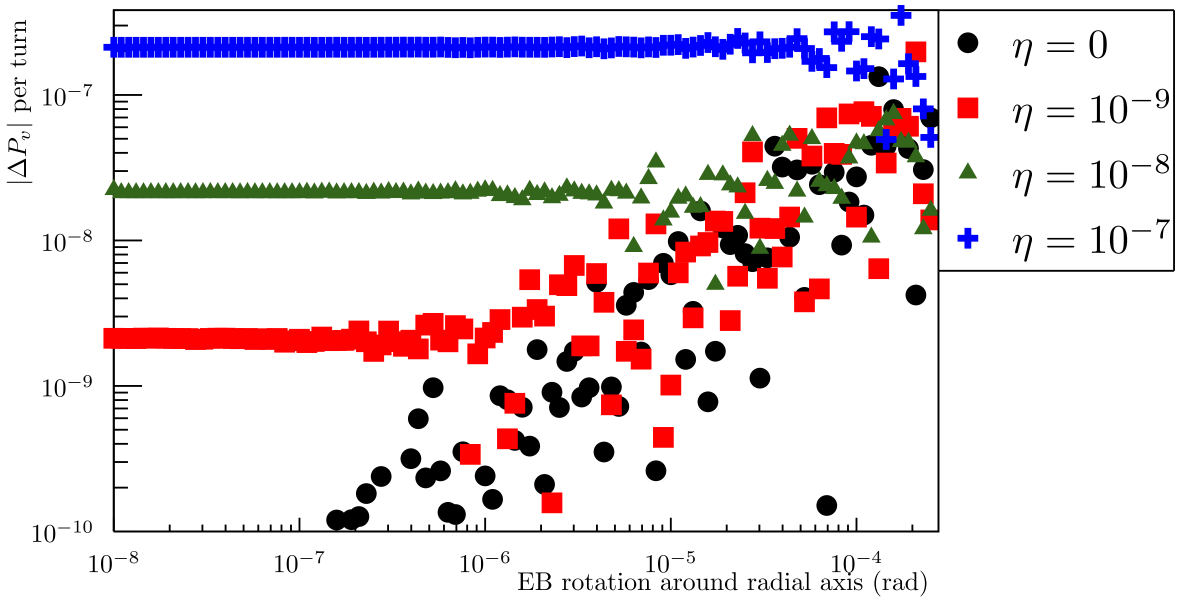

(a) Frozen Spin simulation.

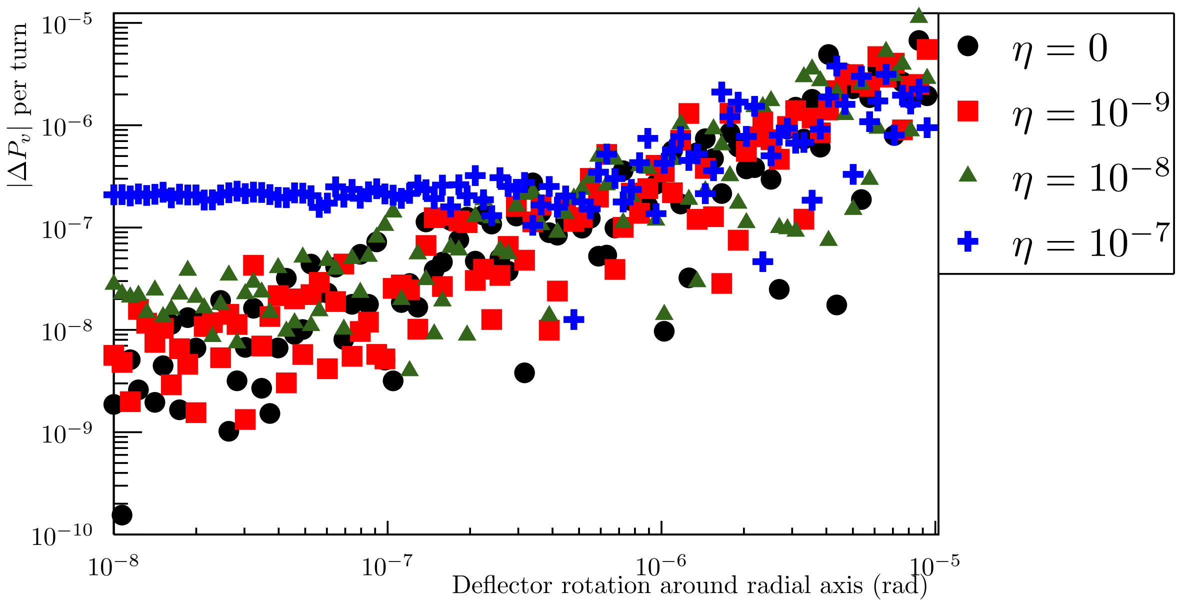

(b) Quasi Frozen Spin simulation.

Figure 5.5: Vertical spin build up for different magnitudes of EDM and RMS of rotation misalignments of the deflectors around the radial axis. Each simulation has new randomly generated misalignments.

5.2.2 Misalignments of Quadrupoles

Shifts Vertical Axis

If quadrupoles are shifted in vertical direction transverse magnetic fields disturb the spin motion (Section 3.3.1). This is confirmed by the simulations shown in Figure 5.6a for the Frozen Spin concept. This kind of misalignments is nearly a magnitude smaller than the effect of rotation misalignments of deflectors around the longitudinal axis (5.4).
The results for shifts of the quadrupoles in the Quasi Frozen ring are the same as for the Frozen Spin. Hence, vertical shifts of the quadrupoles disturb the measurement as in Figure 5.6b are presented.

Shifts Radial Axis

Opposite to the vertical shifts of quadrupoles radial shifts do not effect the spin motion as the simulations, shown in Figure 5.7a, for the Frozen Spin lattice verify.
Figure 5.7b presents the results for the Quasi Frozen Lattice. This kind of misalignments can also be neglected.

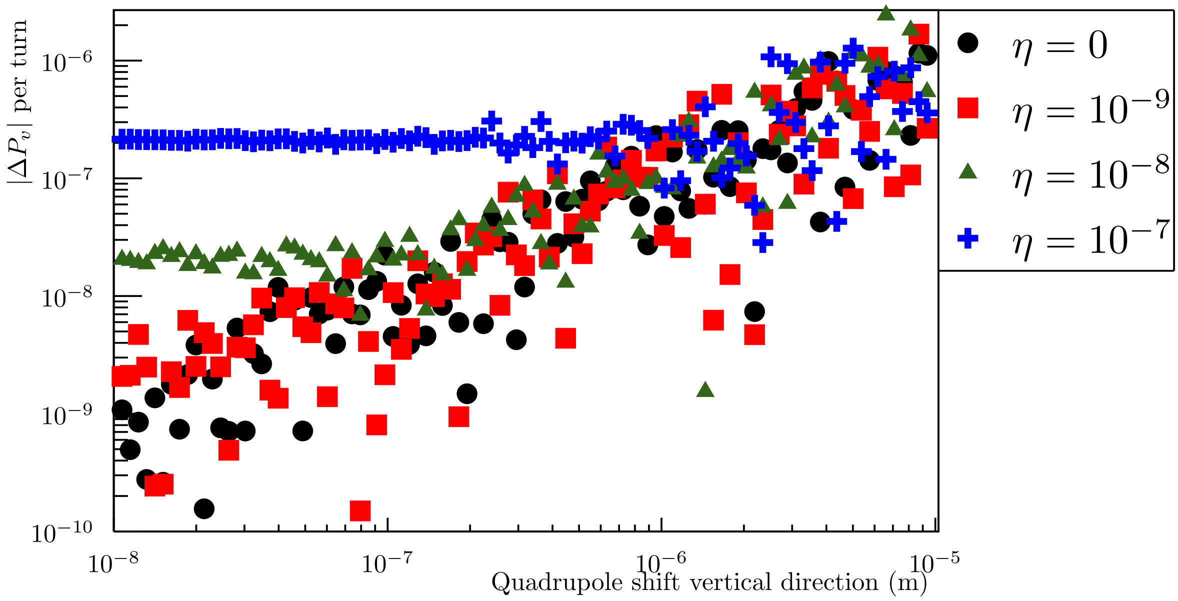

(a) Frozen Spin simulation.

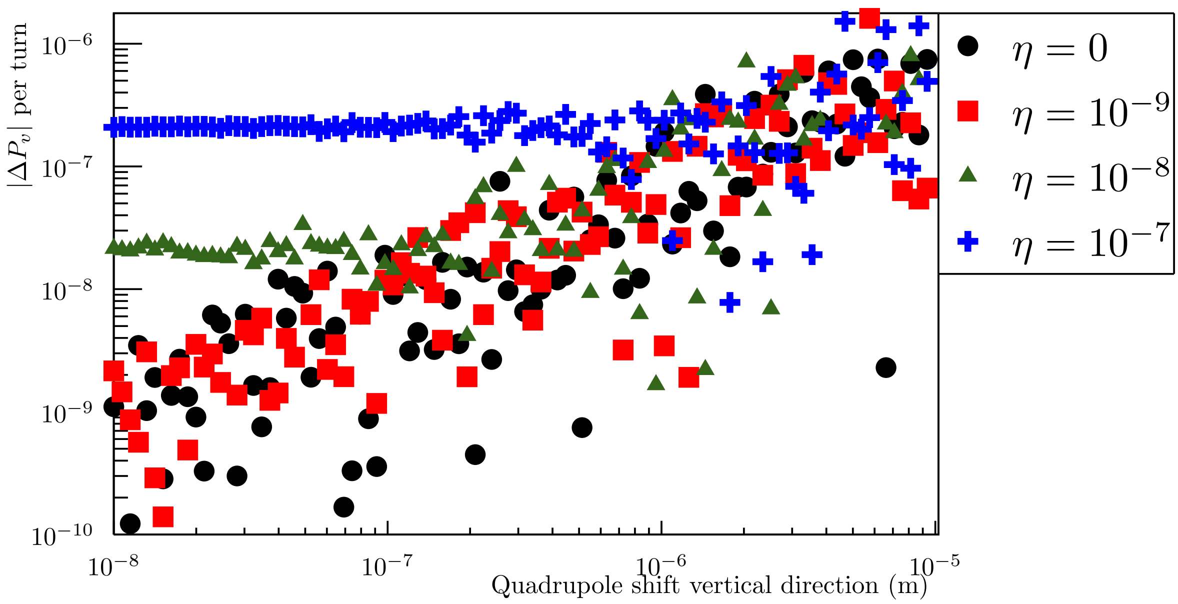

(b) Quasi Frozen Spin simulation.

Figure 5.6: Vertical spin build up for different magnitudes of EDM and RMS of shift misalignments of the quadrupoles in vertical direction. Each simulation has new randomly generated misalignments.

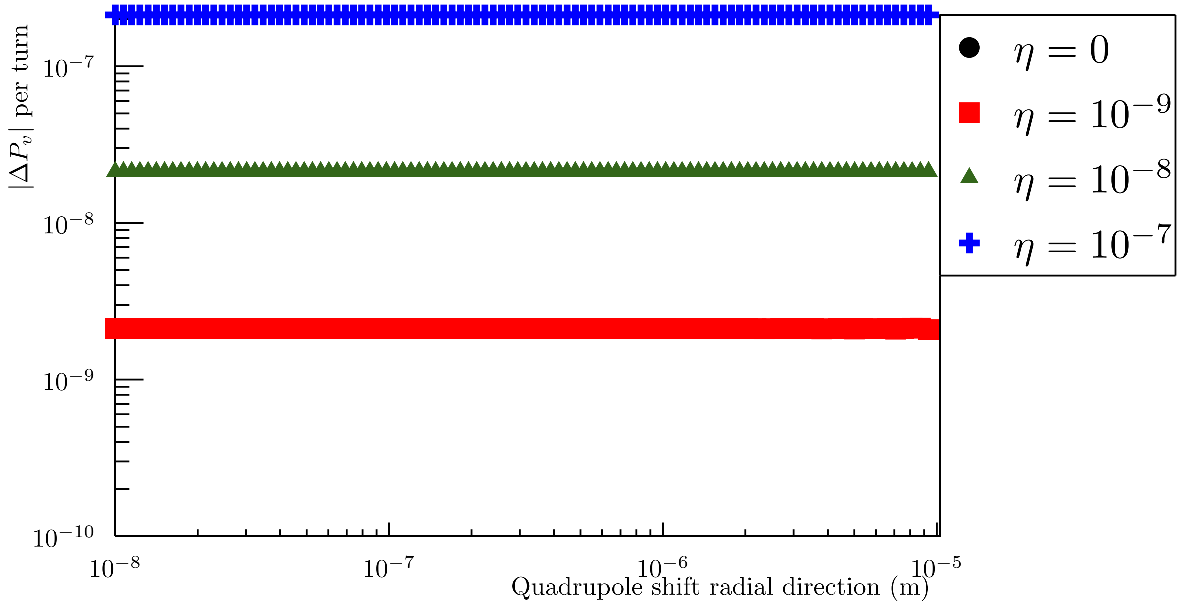

(a) Frozen Spin simulation.

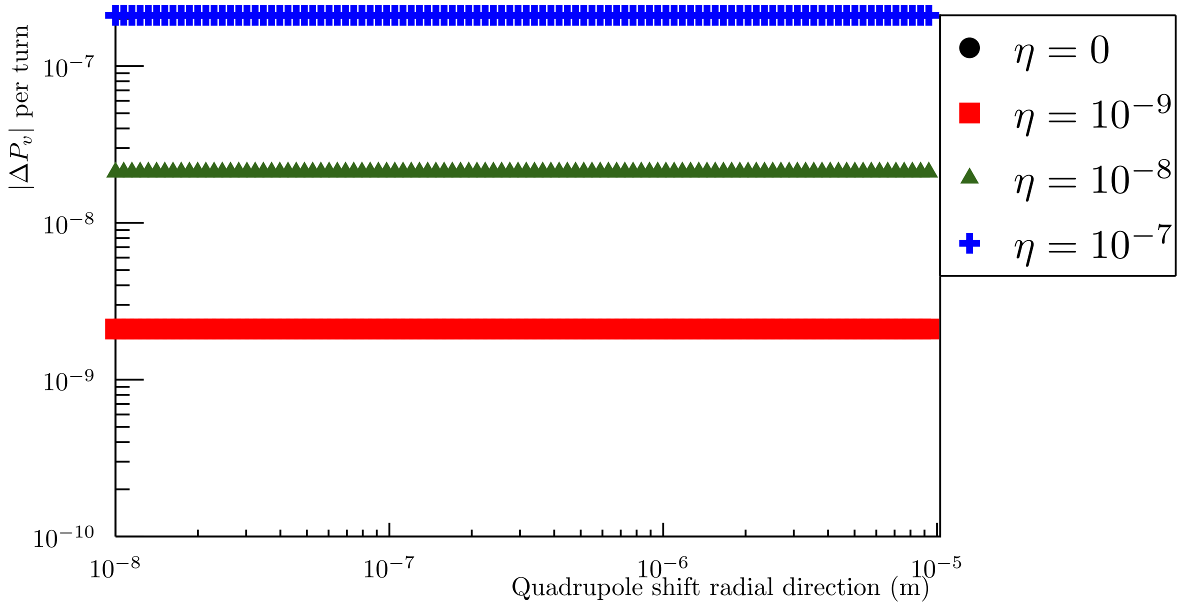

(b) Quasi Frozen Spin simulation.

Figure 5.7: Vertical spin build up for different magnitudes of EDM and RMS of shift misalignments of the quadrupoles in radial direction. Each simulation has new randomly generated misalignments.

5.3 Clockwise Counterclockwise

This section contains the simulation results regarding the CW-CCW method. Deviations for the CW-CCW beam can appear due to limited number of simulated particles. Another serious reason is the modification of the spin invariant axis due to misalignments. For each analysed CW-CCW simulation a set of Gaussian random distributed numbers is generated and only the RMS values of this distribution is modified. Thus a linear dependency on the the vertical Polarisation build up caused by a misalignment and the RMS value is expected (compare Figure 5.10a).
For each misalignments η is extracted. Therefore the results of Section 5.1 are applied. Moreover, for all RMS values a linear fit for the ηs is applied

$$\eta = \eta_0 + \alpha \cdot \text{RMS}. \tag{5.3}$$

All in all the CW-CCW method enables the extraction of the magnitude of η for the simulated misalignments for both kind of rings. However, a simulation of CW-CCW method for rotations of deflector around the radial axis remains. Furthermore it was assumed that the switch of the direction of the magnetic field is perfect. Thus errors regarding the switching of the magnetic fields must be simulated.
Two CW-CCW simulations are exemplary discussed. Section 5.3.1 includes the CW-CCW simulation results of rotation misalignments of E×B deflectors around the vertical axis of the Frozen Spin lattice. The influence of this misalignment on the spin motion is negligible and the spin motion for both directions seems to be the same regarding Figure 5.8a. In Figure 5.8b η is determined. The resulting values of η_0 confirm the above assumption.
Another example of the CW-CCW method is presented in section 5.3. This section contains the result for rotations misalignments around the longitudinal axis of the Frozen Spin lattice. This kind of misalignment influence the spin motion. Thus a linear dependence of the RMS value of misalignments is observed (Figure 5.10a). Figure 5.10b shows the extraction of η of this simulation.
The main reason for different spin motion results of the CW and CCW beam is that all simulations include an initial polarization parallel aligned to the beam direction. However, the invariant spin axis can be rotated by misalignments. Hence, the spin invariant axis can obtain different directions for the CW and CCW beam which results in different observed spin motion if the beam is always parallel aligned to the beam direction.

5.3.1 Misalignments of Deflectors

Rotations around Vertical Axis

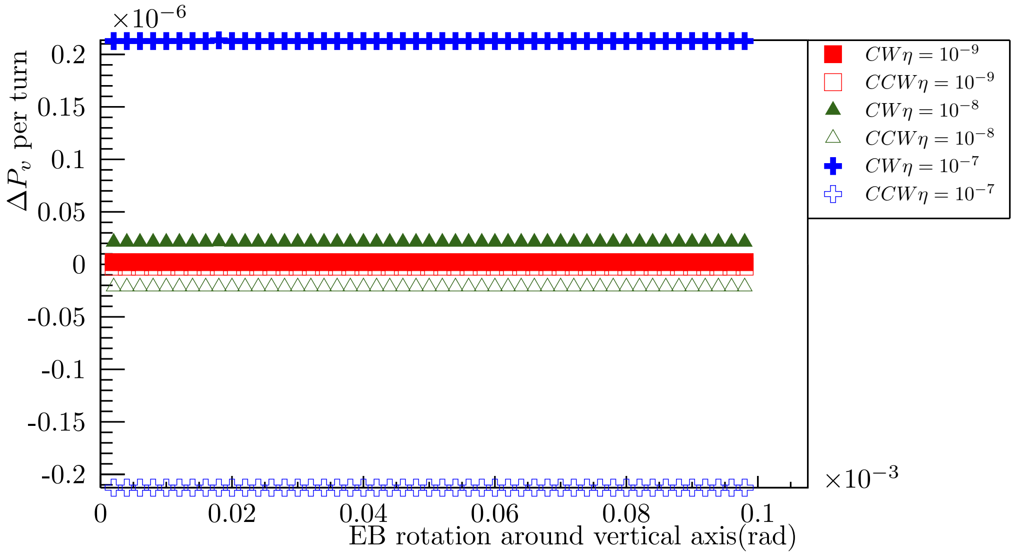

(a) Vertical spin build up for different magnitudes of EDM and RMS of rotation misalignments of the deflectors around the vertical axis.

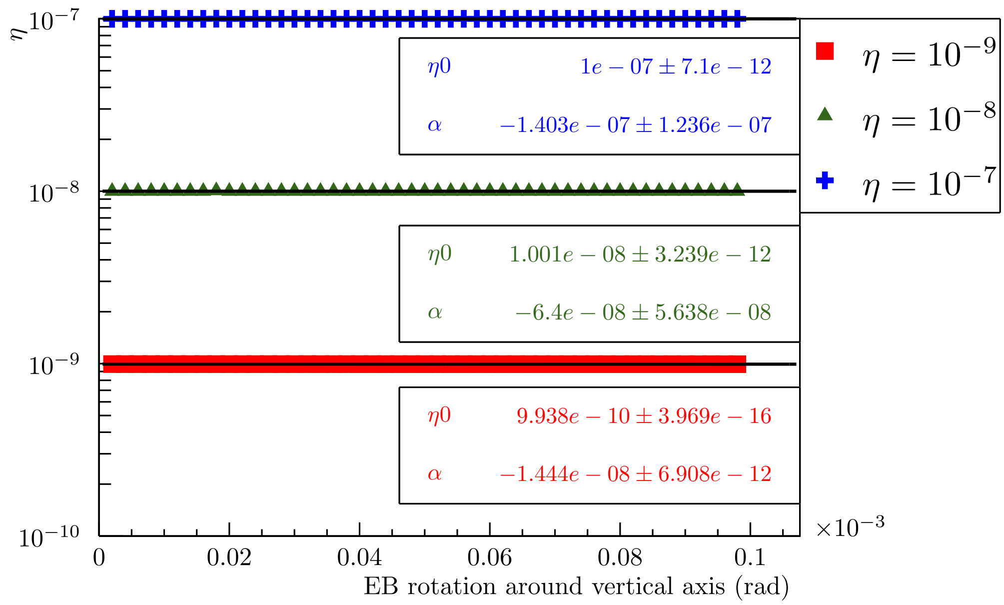

(b) Extracted η for different magnitudes of EDM and RMS of different magnitudes of rotation misalignments of the deflectors around the vertical axis.

Figure 5.8: Frozen Spin - CW-CCW method for rotation misalignments of the E×B deflectors around the vertical axis.

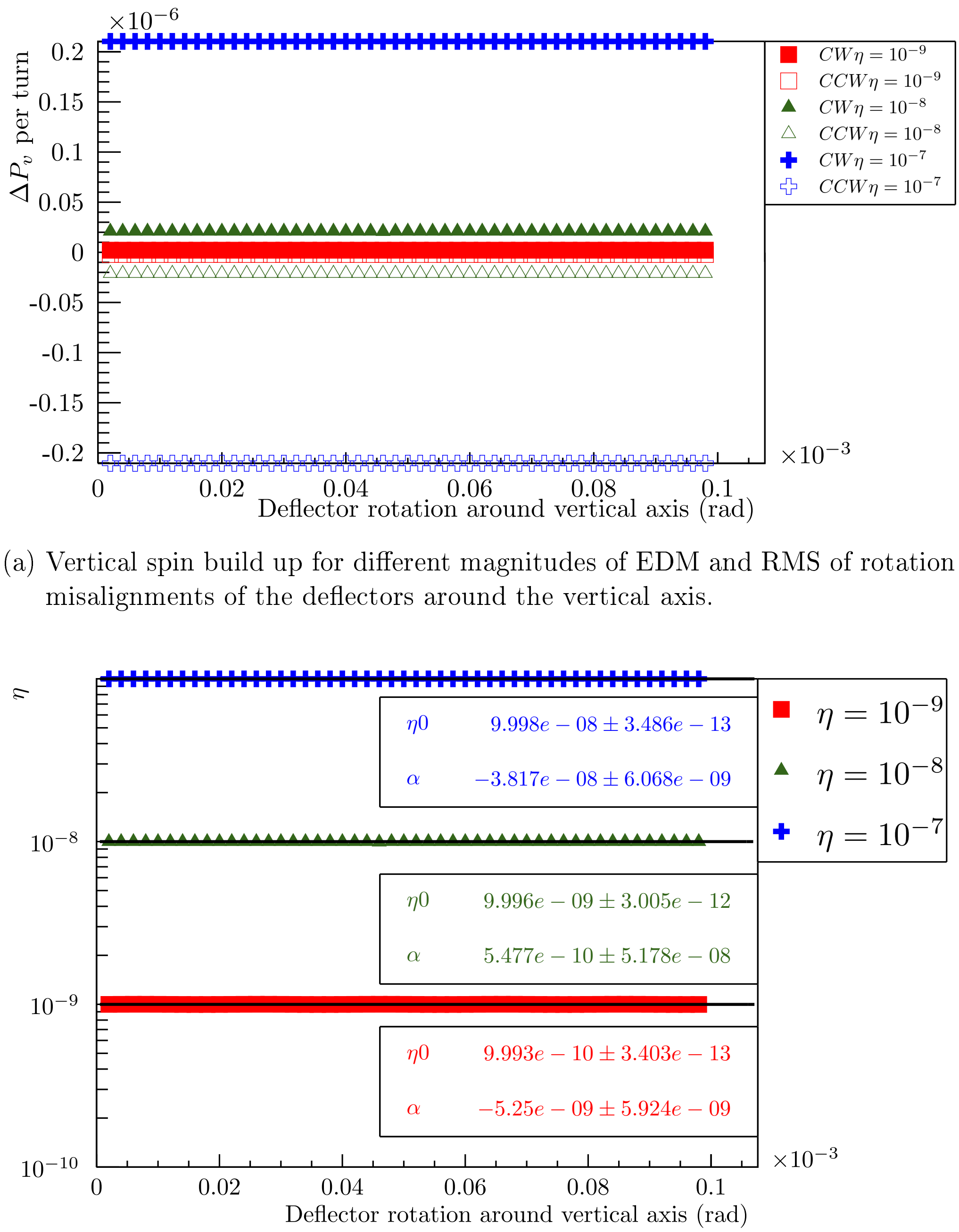

(a) Vertical spin build up for different magnitudes of EDM and RMS of rotation misalignments of the deflectors around the vertical axis.

(b) Extracted η for different magnitudes of EDM and RMS of different magnitudes of rotation misalignments of the deflectors around the vertical axis.

Figure 5.9: Quasi Frozen Spin - CW-CCW method for rotation misalignments of the deflectors around the vertical axis.

Rotations around Longitudinal Axis

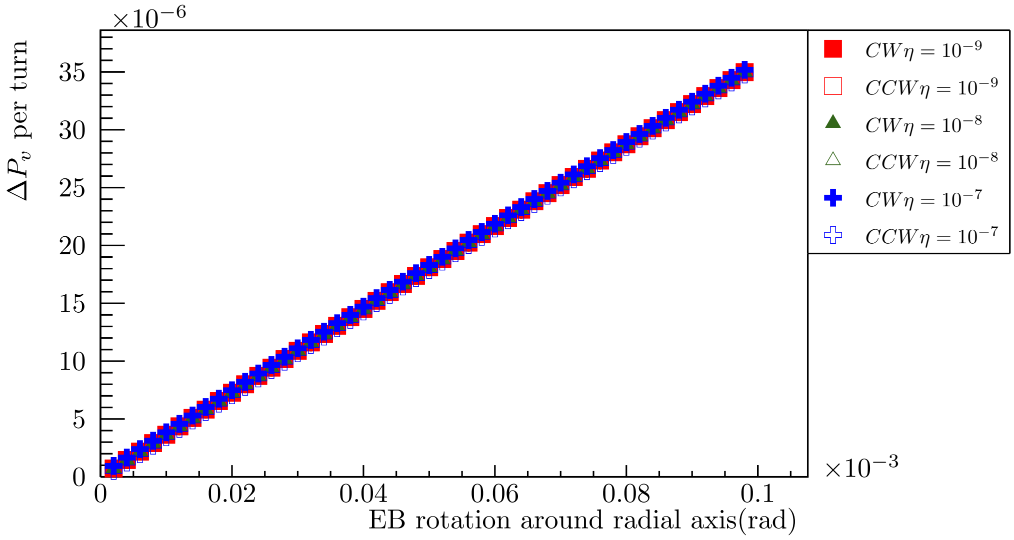

(a) Vertical spin build up for different magnitudes of EDM and RMS of rotation misalignments of the deflectors around the longitudinal axis.

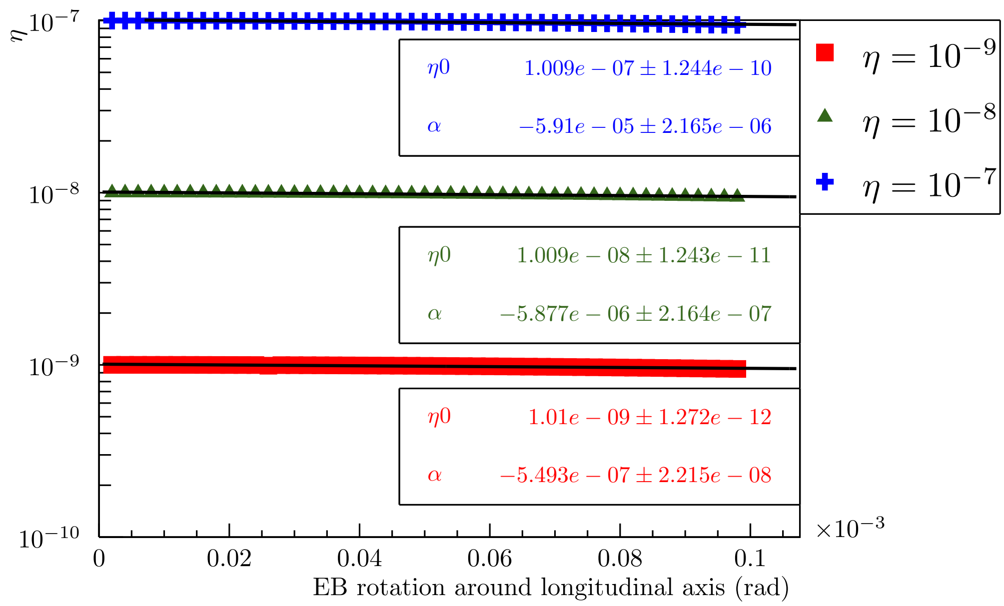

(b) Extracted η for different magnitudes of EDM and RMS of different magnitudes of rotation misalignments of the deflectors around the longitudinal axis.

Figure 5.10: Frozen Spin - CW-CCW method for rotation misalignments of the deflectors around the longitudinal axis.

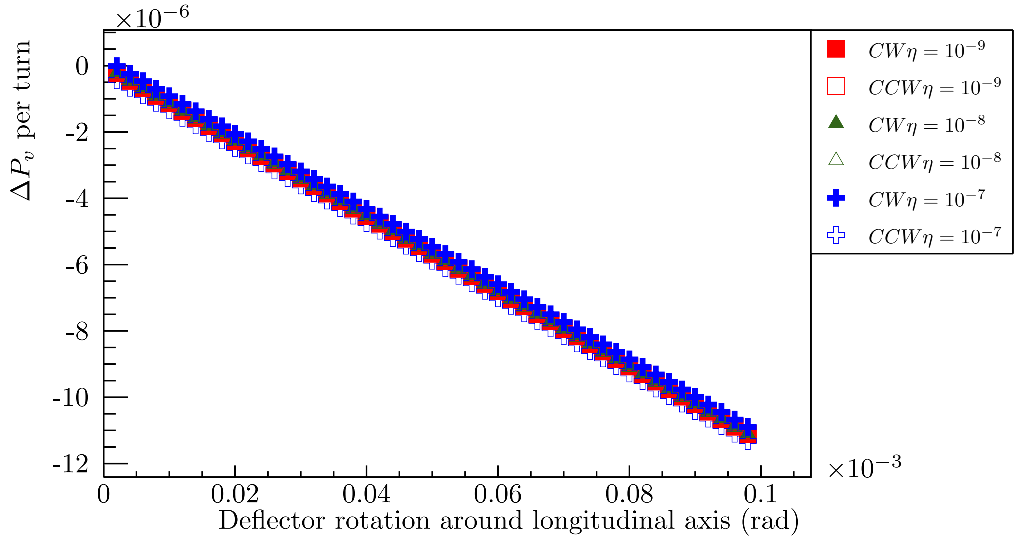

(a) Vertical spin build up for different magnitudes of EDM and RMS of rotation misalignments of the deflectors around the longitudinal axis.

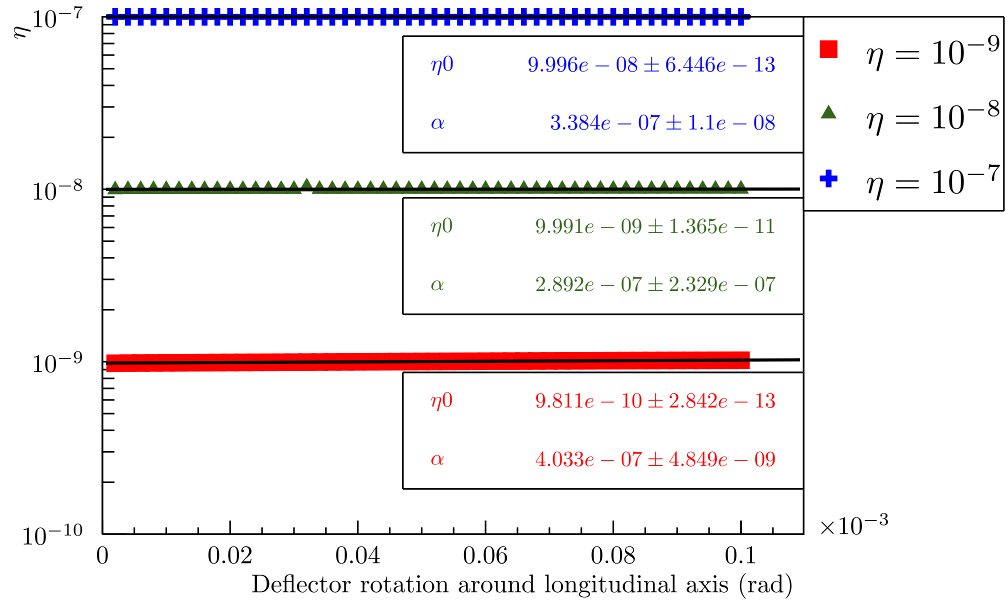

(b) Extracted η for different magnitudes of EDM and RMS of different magnitudes of rotation misalignments of the deflectors around the longitudinal axis.

Figure 5.11: Quasi Frozen Spin - CW-CCW method for rotation misalignments of the deflectors around the longitudinal axis.

5.3.2 Misalignments of Quadrupoles

Shifts Vertical Axis

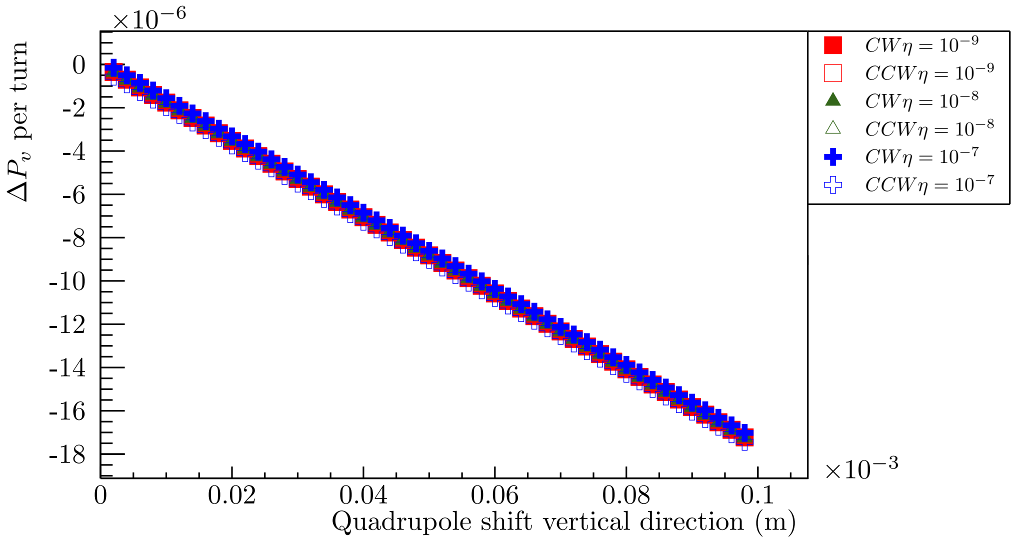

(a) Vertical spin build up for different magnitudes of EDM and RMS of shift misalignments of the quadrupoles in vertical direction.

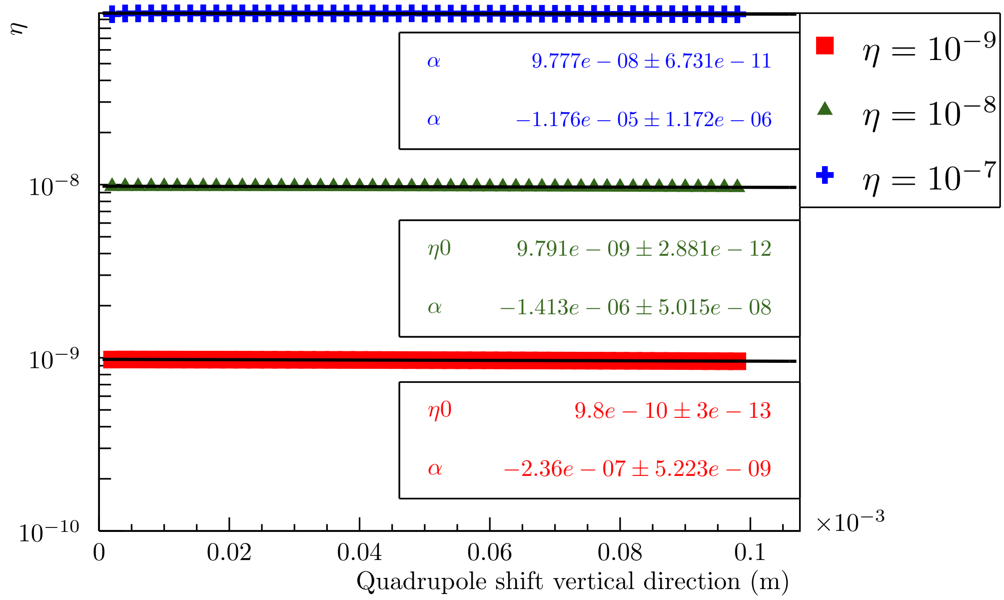

(b) Extracted η for different magnitudes of EDM and RMS of different magnitudes of shift misalignments of the quadrupoles in vertical direction.

Figure 5.12: Frozen Spin - CW-CCW method for shift misalignments of the quadrupoles in vertical direction.

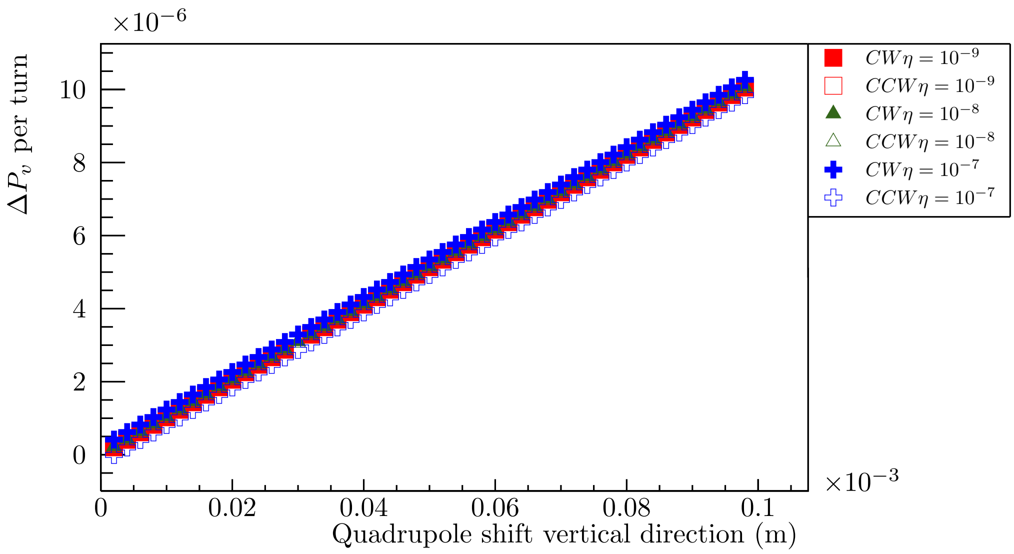

(a) Vertical spin build up for different magnitudes of EDM and RMS of shift misalignments of the quadrupoles in vertical direction.

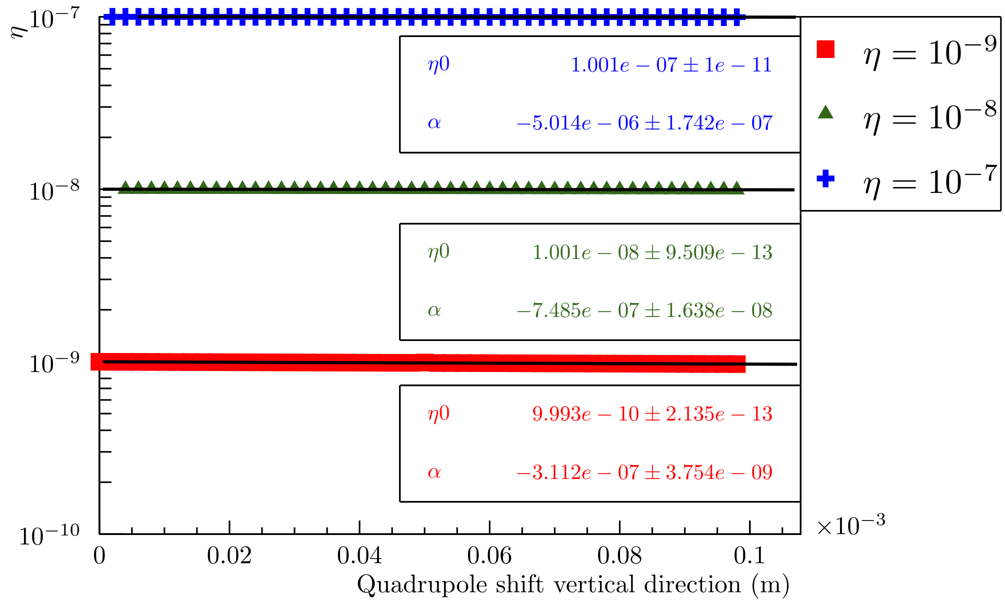

(b) Extracted η for different magnitudes of EDM and RMS of shift misalignments of the quadrupoles in vertical direction.

Figure 5.13: Quasi Frozen Spin - CW-CCW method for shift misalignments of the quadrupoles in vertical direction.

Shifts Radial Axis

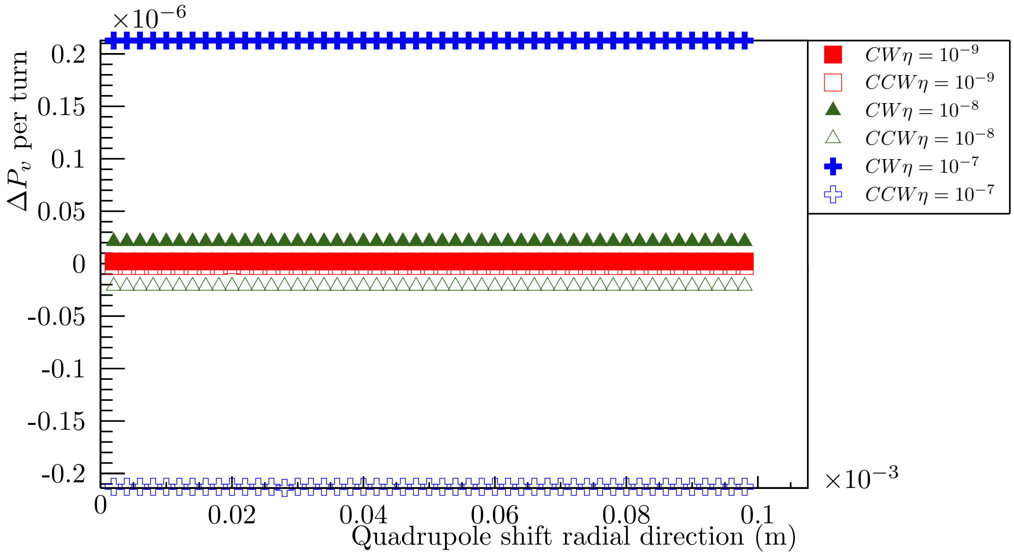

(a) Vertical spin build up for different magnitudes of EDM and RMS of shift misalignments of the quadrupoles in radial direction.

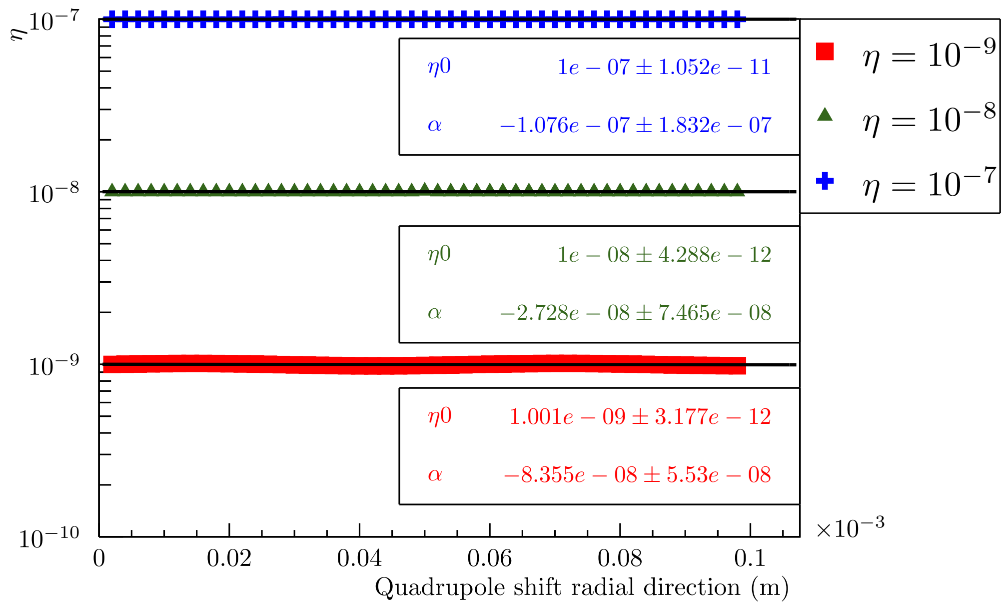

(b) Extracted η for different magnitudes of EDM and RMS of different magnitudes of shift misalignments of the quadrupoles in radial direction.

Figure 5.14: Frozen Spin - CW-CCW method for shift misalignments of the quadrupoles in radial direction.

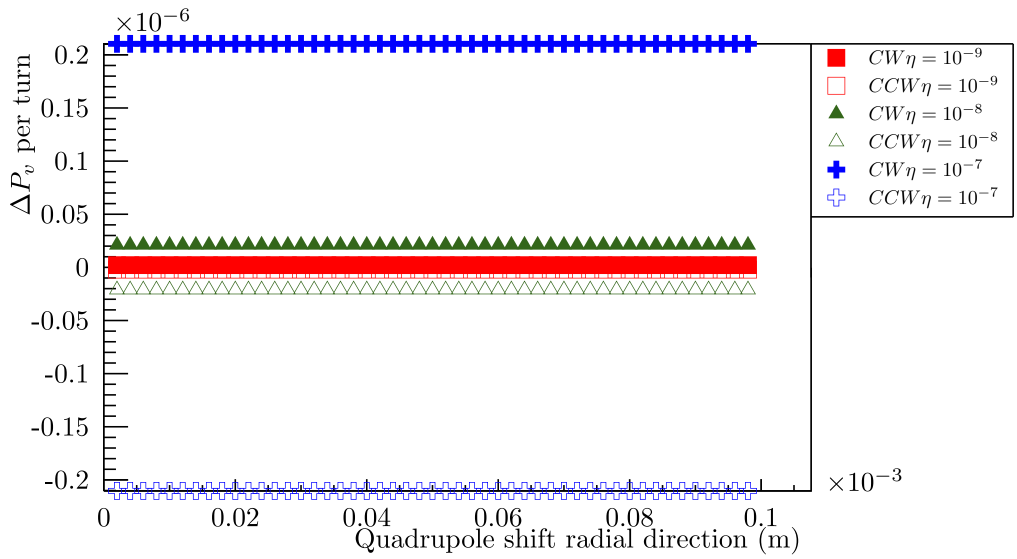

(a) Vertical spin build up for different magnitudes of EDM and RMS of shift misalignments of the quadrupoles in radial direction.

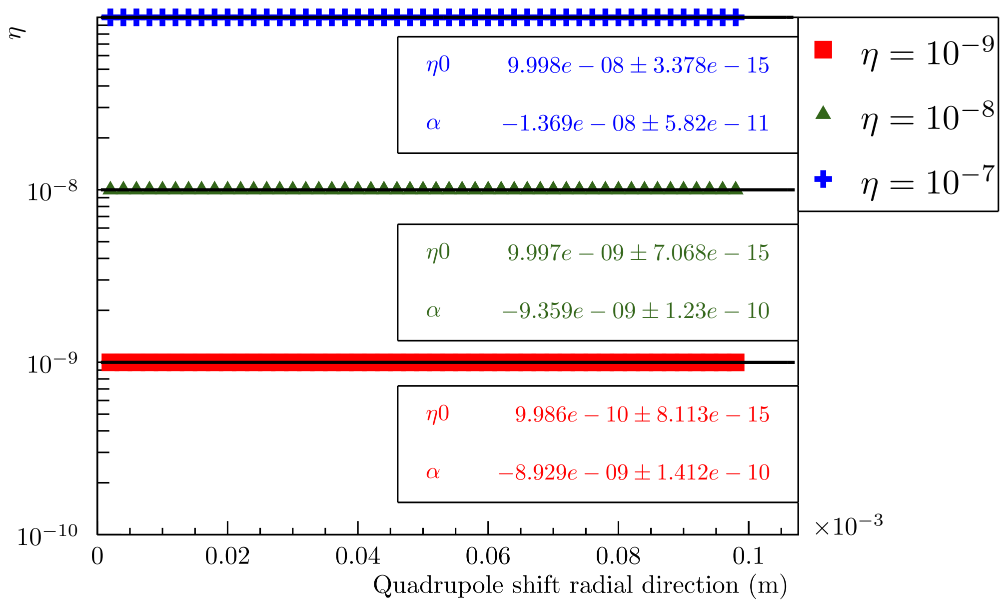

(b) Extracted η for different magnitudes of EDM and RMS of shift misalignments of the quadrupoles in radial direction.

Figure 5.15: Quasi Frozen - CW-CCW method for shift misalignments of the quadrupoles in radial direction.

6 Summary and Outlook

Different systematic effects regarding the EDM measurement are analysed in Section 3.3. The uncorrected influence of gravitation prohibits an EDM measurement. The influence of gradient fields in the Frozen Spin lattice is negligible compared to the influence in the Quasi Frozen Spin lattice. Hence more detailed simulations are required to analyse exactly this effect. Furthermore misalignments are discussed and accompanying simulations confirm the analysis results (Section 5.2). Relating to the misalignments the largest difference between Frozen and Quasi Frozen spin are longitudinal fields. Due to the orientation of the polarization parallel aligned to the beam motion longitudinal fields do not disturb the spin motion in the Frozen Spin concept in comparison to the Quasi Frozen Spin concept (Section 3.3.3, 5.2.1).
COSY Toolbox is enhanced with necessary tools to enable the simulation of the final EDM storage rings (Chapter 4). E×B deflectors and sector magnets are included and calculators for the properties of EDM storage ring are adjusted. Additionally, the lattices of two possible drafts of EDM storage rings are included and are simulated. Analyse tools for the spin behaviour are integrated. During is discussed that COSY INFINITY is not the optimal tool to simulate devices with complete 3D field maps (Section 4.3.1). This would be necessary to enable the simulation and test of the effect of curved E×B deflectors on the EDM. Moreover, COSY Toolbox includes the parameters for electrical fringe fields, now.
It is proved that for a perfect ring without misalignments the Frozen and Quasi Frozen Spin concept works. However, unavoidable misalignments in the ring prevent a measurement of the EDM (Section 5.2). Hence, corrective actions are essential. In connection with this the CW-CCW method, assuming a perfect reverse of the magnetic fields, is a certified possibility to handle the errors caused by rotations of the deflectors around the vertical and longitudinal axis (Section 5.3). Furthermore this method corrects the misleading effect by shifts of quadrupoles.
All in all Frozen Spin has advantages with different kind of misalignments and artificial vertical spin build up due to the fact that the spin is frozen in comparison with the Quasi Frozen spin method (Section 3.3.2, 3.3.3, 5.2). The choice of the polarization in beam direction benefits by the fact that this direction of polarization does not see many possible negative influences as longitudinal electromagnetic fields or the gradient field in an accelerator.
A possibility to minimise the error in Quasi Frozen Ring concept would be to decrease

the desired deflection of spin direction. E.g. a Quasi Frozen Ring should not contain two arcs with magnetic deflectors and two lines with correctors for the deflection of the polarization. The lattice construction should be changed in such a way that a lot of pairs of magnetic deflectors and a correction elements like E×B deflectors are used.
To make a final decision between Frozen and Quasi Frozen Spin it is unavoidable to use integration algorithms to simulate all effects of curved E×B deflectors. Regarding the CW-CCW method the applicability must be checked, if the reverse of the magnetic fields is not perfect.

Bibliography

[1] A. Sakharov. Violation of CP invariance, C asymmetry, and baryon asymmetry of the universe. *JETP lett.*, 5:24–27, 1967.

[2] A. Wirzba. Electric dipole moments of the nucleon and light nuclei . *Nuclear Physics A*, 928:116 – 127, 2014. ISSN 0375-9474. doi: http://dx.doi.org/10.1016/j.nuclphysa.2014.04.003. URL http://www.sciencedirect.com/science/article/pii/S0375947414000852. Special Issue Dedicated to the Memory of Gerald E Brown (1926-2013).

[3] A. Lehrach et al. Precursor experiments to search for permanent Electric Dipole Moments (EDMs) of protons and deuterons at COSY. *arXiv preprint arXiv:1201.5773*, 2012.

[4] D. Anastassopoulos, EDM Collaboration, et al. AGS Proposal: Search for a permanent electric dipole moment of the deuteron nucleus at the 10^{-29} ecm level. *BNL Report*, 2008.

[5] Y. Senichev et al. Investigation of lattice for deuteron EDM ring. *ICAP 2015, Shanghai, China*, 2015.

[6] M. Berz et al. *COSY INFINTIY 9.2 Beam Physics Manual*, 2015.

[7] M. Rosenthal. Development of a new control framework for lattice parameter calculations and particle tracking. *Annual Report, Jülich Center for Hadron Physics*, 2014.

[8] D. Spergel et al. First-Year Wilkinson Microwave Anisotropy Probe (WMAP) Observations: Determination of Cosmological Parameters. *The Astrophysical Journal Supplement Series*, 148(1):175, 2003. URL http://stacks.iop.org/0067-0049/148/i=1/a=175.

[9] W. Bernreuther. CP violation and baryogenesis. In *CP Violation in Particle, Nuclear and Astrophysics*, pages 237–293. Springer, 2002.

[10] F. Rathmann et al. Search for electric dipole moments of light ions in storage rings. *Physics of particles and nuclei*, 45(1):229–233, 2014.

[11] D. Anastassopoulos, EDM Collaboration, et al. A Proposal to Measure the Proton Electric Dipole Moment with 10-29e cm Sensitivity by the Storage Ring EDM Collaboration. *BNL Report*, 2011.

[12] I. Altarev et al. Towards a new measurement of the neutron electric dipole moment. *Nuclear Instruments and Methods in Physics Research Section A: Accelerators, Spectrometers, Detectors and Associated Equipment*, 611(2):133–136, 2009.

[13] L. Thomas. The motion of the spinning electron. *Nature*, 117:514, 1926.

[14] L. Thomas. I. The kinematics of an electron with an axis. *The London, Edinburgh, and Dublin Philosophical Magazine and Journal of Science*, 3(13):1–22, 1927.

[15] V. Bargmann et al. Precession of the polarization of particles moving in a homogeneous electromagnetic field. *Physical Review Letters*, 2(10):435, 1959.

[16] E. Metodiev. Thomas-BMT equation generalized to electric dipole moments and field gradients. *arXiv preprint arXiv:1507.04440*, 2015.

[17] W. Gerlach et al. Das magnetische Moment des Silberatoms. *Zeitschrift für Physik*, 9(1):353–355, 1922. ISSN 0044-3328. doi: 10.1007/BF01326984. URL http://dx.doi.org/10.1007/BF01326984.

[18] T. Fukuyama et al. Derivation of generalized Thomas–Bargmann–Michel–Telegdi equation for a particle with electric dipole moment. *International Journal of Modern Physics A*, 28(29):1350147, 2013.

[19] Y. Orlov et al. Spin rotation by Earth$\hat{\mathrm{E}}\frac{1}{4}$s gravitational field in a frozen-spin ring. *Physics Letters A*, 376(45):2822–2829, 2012. URL http://www.sciencedirect.com/science/article/pii/S0375960112008973/pdfft?md5=9154dd6c9679fd064fce291466972d39&pid=1-s2.0-S0375960112008973-main.pdf.

[20] A Einstein. Die feldgleichungen der gravitation sitzungsberichte der preußischen akademie der wissenschaften zu berlin: 844–847. *2006) Albert Einstein: Akademie-Vortrage: Sitzungsberichte der Preußischen Akademie der Wissenschaften*, 1932, 1914.

[21] D. Anastassopoulos et al. A storage ring experiment to detect a proton electric dipole moment. *arXiv preprint arXiv:1502.04317*, 2015.

[22] A. Lehrach. Beam and Spin Dynamics for Storage Ring Based EDM Search. *Sixth International Particle Accelerator Conference*, 2015.

[23] G Guidoboni on behalf of the JEDI Collaboration. Spin coherence time studies of a horizontally polarized deuteron beam at COSY. *Physica Scripta*, 2015(T166): 014036, 2015. URL http://stacks.iop.org/1402-4896/2015/i=T166/a=014036.

[24] J.Pretz. Statistical Error of an EDM measurement with an RF-Wien filter. *Private Note*, 2013.

[25] J. Pretz. Measurement of permanent electric dipole moments of charged hadrons in storage rings. *Hyperfine Interactions*, 214(1):111–117, 2013. ISSN 1572-9540. doi: 10.1007/s10751-013-0799-4. URL http://dx.doi.org/10.1007/s10751-013-0799-4.

[26] K. Olive et al. Review of Particle Physics. *Chin. Phys.*, C38:090001, 2014. doi: 10.1088/1674-1137/38/9/090001.

[27] P. Mohr et al. CODATA Recommended Values of the Fundamental Physical Constants: 2014. *ArXiv e-prints*, July 2015.

[28] Y. Senichev. Private Communications. 2016.

[29] A. Skawran. Manual - COTOBO Extensions for EDM Storage Ring Simulations. *unpublished*, 2016.

[30] Y. Senichev et al. Quasi-frozen Spin Method for EDM Deuteron Search. *Proceedings of IPAC2015*, 2015.

[31] MATLAB and Statistics Toolbox Release 2016a, The MathWorks, Inc., Natick, Massachusetts, United States., 2016.

[32] L. Shampine et al. The matlab ode suite. *SIAM journal on scientific computing*, 18(1):1–22, 1997.

[33] M. Rosenthal. Investigation of Beam and Spin Dynamics for EDM Measurements at COSY. *Microscopy and Microanalysis*, 21(S4):30–35, 2015.

[34] M. Berz. *Modern map methods in particle beam physics*, volume 108. Academic Press, 1999.

[35] K. Makino et al. Cosy infinity version 9. *Nuclear Instruments and Methods in Physics Research Section A: Accelerators, Spectrometers, Detectors and Associated Equipment*, 558(1):346–350, 2006.

[36] R. Brun et al. ROOT-an object oriented data analysis framework. *Nuclear Instruments and Methods in Physics Research Section A: Accelerators, Spectrometers, Detectors and Associated Equipment*, 389(1):81–86, 1997.

[37] B. Bellenot et al. ROOT 6 and beyond: TObject, C++14 and many cores. *Journal of Physics: Conference Series*, 664(6):062006, 2015. URL http://stacks.iop.org/1742-6596/664/i=6/a=062006.

[38] M. Rosenthal. Software framework: COSY Toolbox. *Annual Report, Jülich Center for Hadron Physics*, 2015.

[39] E. Metodiev et al. Fringe electric fields of flat and cylindrical deflectors in electrostatic charged particle storage rings. *Physical Review Special Topics-Accelerators and Beams*, 17(7):074002, 2014.

[40] J. Maxwell. *A treatise on electricity and magnetism*, volume 1. Clarendon press, 1881.

[41] E. Valetov. Private Communications. 2016.

[42] A. Skawran et al. Extension of COSY Toolbox for the Analysis of the Final Electric Dipole Moment Storage Ring. *Annual Report, Jülich Center for Hadron Physics*, 2016.

[43] C. Hoare. Quicksort. *The Computer Journal*, 5(1):10–16, 1962.

Acknowledgements

I want express thanks to the people who supported my work.
Thanks to my supervisor Prof. Dr. Andreas Lehrach who introduced me to accelerator physics by his lecture and the informative talks regarding my thesis.
Many thanks to the developer of COSY Toolbox Marcel Rosenthal who always found some time to explain details of his framework and for the inspiring conversations.
Furthermore I want to thank Eremey Valetov for his advices and discussions regarding the use of COSY INFINITY and the fringe fields.
Thanks to Yuri Senichev who developed both simulated ring lattices.
Many thanks for the high-calorie support by Vera Schmidt. Besides I thank Bernd Lorentz, Dennis Eversmann, Fabian Hinder, Fabian Trinkel, Frank Rathmann, Jan Hetzel, Jörg Pretz and Volker Hejny for their comments and advices.
Furthermore I express thanks to my family and all my friends who supported me during my studies at the RWTH Aachen.

7 Statutory Declaration / Eidesstattliche Versicherung

Eidesstattliche Versicherung

Name, Vorname

Matrikelnummer (freiwillige Angabe)

Ich versichere hiermit an Eides Statt, dass ich die vorliegende Arbeit/Bachelorarbeit/ Masterarbeit* mit dem Titel

selbständig und ohne unzulässige fremde Hilfe erbracht habe. Ich habe keine anderen als die angegebenen Quellen und Hilfsmittel benutzt. Für den Fall, dass die Arbeit zusätzlich auf einem Datenträger eingereicht wird, erkläre ich, dass die schriftliche und die elektronische Form vollständig übereinstimmen. Die Arbeit hat in gleicher oder ähnlicher Form noch keiner Prüfungsbehörde vorgelegen.

Ort, Datum

Unterschrift

*Nichtzutreffendes bitte streichen

Belehrung:

§ 156 StGB: Falsche Versicherung an Eides Statt

Wer vor einer zur Abnahme einer Versicherung an Eides Statt zuständigen Behörde eine solche Versicherung falsch abgibt oder unter Berufung auf eine solche Versicherung falsch aussagt, wird mit Freiheitsstrafe bis zu drei Jahren oder mit Geldstrafe bestraft.

§ 161 StGB: Fahrlässiger Falscheid; fahrlässige falsche Versicherung an Eides Statt

(1) Wenn eine der in den §§ 154 bis 156 bezeichneten Handlungen aus Fahrlässigkeit begangen worden ist, so tritt Freiheitsstrafe bis zu einem Jahr oder Geldstrafe ein.

(2) Straflosigkeit tritt ein, wenn der Täter die falsche Angabe rechtzeitig berichtigt. Die Vorschriften des § 158 Abs. 2 und 3 gelten entsprechend.

Die vorstehende Belehrung habe ich zur Kenntnis genommen:

Ort, Datum

Unterschrift